Faculty of Chemical Technology

Inorganic Materials Science

Final Report

University of Twente
university for technical and
social sciences

Pt, Au and Ag Electrodes on BiCuVOx

(under contract F61708-97-W0049)

Bernard A. Boukamp

University of Twente

Inorganic Materials Science

P.O. Box 217

7500 AE Enschede

The Netherlands

April-December 1997

98·484/CT31/bab 28 August 1998

REPORT DOCUMENTATION PAGE

Form Approved OMB No. 0704-0188

1. AGENCY USE ONLY (Leave blank)	2. REPORT DATE	3. REPORT TYPE AND DATES COVERED
	28 August 1998	Final Report

4. TITLE AND SUBTITLE

Pt, Au and Ag Electrodes on BiCuVOx

5. FUNDING NUMBERS

F6170897W0049

6. AUTHOR(S)

Dr. Bernard Abraham Boukamp

7. PERFORMING ORGANIZATION NAME(S) AND ADDRESS(ES)

University of Twente
Faculty of Chemical Technology
P.O. Box 217
Enschede 7500 AE
Netherlands

8. PERFORMING ORGANIZATION REPORT NUMBER

N/A

9. SPONSORING/MONITORING AGENCY NAME(S) AND ADDRESS(ES)

EOARD
PSC 802 BOX 14
FPO 09499-0200

10. SPONSORING/MONITORING AGENCY REPORT NUMBER

SPC 97-4031

11. SUPPLEMENTARY NOTES

12a. DISTRIBUTION/AVAILABILITY STATEMENT

Approved for public release; distribution is unlimited.

12b. DISTRIBUTION CODE

A

13. ABSTRACT (Maximum 200 words)

Impedance spectra of a porous Pt, Au and Ag electrode on $Bi_2Cu_{0.1}V_{0.9}O_{5.35}$ (BiCuVOx) were studied as function of temperature (200° to 735° C), oxygen partial pressure and polarization level. Also, dc polarization curves (I-V) were measured at intermediate (473° C) and high (735°) temperature. At low temperature (<500°) the electrode response is slow, characterized by hysteresis in the I-V curves. The impedance spectra of Pt and Au electrodes at low temperature are nearly identical, in contrast with observations for zirconia-based electrodes. High temperature impedance spectra are characterized by a significant contribution of a diffusion type element (Warburg) parallel to a resistance with characteristics of a charge transfer resistance. Both elements show strong dependence on pO_2 and polarization level. Results are explained with theoretical and observational arguments.

14. SUBJECT TERMS

EOARD, Aircraft Subsystem, Chemistry, Materials, oxygen pump, porous electrode, oxygen ion conductivity, oxide electrode

15. NUMBER OF PAGES

36

16. PRICE CODE

N/A

17. SECURITY CLASSIFICATION OF REPORT	18. SECURITY CLASSIFICATION OF THIS PAGE	19. SECURITY CLASSIFICATION OF ABSTRACT	20. LIMITATION OF ABSTRACT
UNCLASSIFIED	UNCLASSIFIED	UNCLASSIFIED	UL

NSN 7540-01-280-5500

Standard Form 298 (Rev. 2-89)
Prescribed by ANSI Std. 239-18
298-102

Abstract

The electrode responses (impedance spectra) of a porous Pt, Au and Ag electrode on $Bi_2Cu_{0.1}V_{0.9}O_{5.35}$ (abbreviated: BiCuVOx) have been studied in the temperature range 200° to 735 °C as function of temperature, oxygen partial pressure and polarisation level. Also 'dc'- polarisation curves (*I-V*) have been measured at intermediate (473 °C) and high (735 °C) temperature. In the low temperature range (<500 °C) the electrode response is slow. The response to polarisation of the electrodes is characterised by considerable hysteresis in the *I-V* curves. The observed behaviour can well be explained by the occurrance of a change in composition (oxygen 'non-stoichiometry') in the electrode surface region. This implies that part of the imposed polarisation is counteracted by a change in the oxygen activity of the bulk at the electrolyte electrode interface, resulting in a diminished driving force for the actual electrode reaction. The impedance spectra of the Pt and Au electrodes on BiCuVOx in the low temperature range are more or less identical, quite in contrast with findings for zirconia based electrode systems.

The high temperature impedance spectra are characterised by a significant contribution of a diffusion type element (Warburg) parallel to a resistance with characteristics of a charge transfer resistance. Both elements show strong dependence on pO_2 and polarisation level. The effects can qualitatively, but consistantly, be explained in terms of a model presented previously for the $Bi_{1.5}Er_{0.5}O_3$/Au, O_2 electrode system. Exchange current densities and activation energies for both the BiCuVOx- and BiEr25-electrode systems are quite comparable.

A consistently found negative (*RC*) contribution in the low frequency region of the impedance spectra could tentatively be explained by the occurrance of 'cross talk' between the working electrode and the reference electrode, possibly mediated by the diffusion of adsorbed, charged oxygen species.

Table of contents

1 Introduction

The family of the so-called BiMeVOx oxides (formula: $Bi_2M_xV_{1-x}O_{5.5-y}$ where M stands for a large variety of metal ions) shows very high oxygen ion conductivity, even at low temperatures. Because of this property these materials have a potential for application in a medium temperature oxygen pump. But besides high ionic conductivity, these materials must also exhibit good oxygen transfer properties at the oxide/electrode interface. Hence the choice of electrode material will be crucial for the optimal performance of an oxygen pump. There are basically two types of electrode systems for oxygen transfer in solid electrolytes, porous (noble) metal electrodes and (porous) mixed conducting oxides, i.e. oxides that show both ionic and electronic conductivity. A prerequisite for these oxide electrodes is that no detrimental reactions may occur between electrode and electrolyte. This possible complication and the difficult application technique preclude the use of mixed conducting oxides in this study. The noble metals (gold, platinum and silver) are much less reactive with most oxides and application on electrolytes can be done by simple, generally available techniques.

For yttria stabilized zirconia (YSZ), a well known high-temperature oxygen electrolyte, it was found that porous platinum electrodes were superior to porous gold electrodes. This is ascribed to the much greater catalytic activity of Pt over Au with respect to the dissociation of absorbed oxygen. Comparable silver electrodes show an even higher activity on YSZ. Unfortunately the Ag-electrode structure is very unstable due to surface diffusion and recrystallisation at high temperatures (700-1000°C).

For some bismuth oxide based electrolyte materials (e.g. the rare earth doped δ-bismuth sesqui-oxides) the difference between porous Pt and Au electrodes was found to be insignificant. A clear relation was observed between exposed electrolyte area (ratio of pore area to macroscopic electrode surface area) and the electrode resistance. Secondly, a relation could be indicated between the mean pore diameter and the frequency scaling of the electrode dispersion. Furthermore the oxygen exchange rate, measured from isotopic exchange experiments could be linked directly to the exchange current density, obtained from polarization measurements for these electrodes [1-5]. Based on these results it was concluded that the exposed electrolyte area, within the macroscopic electrode region is the active area for oxygen- and charge transfer, while the noble metal electrode merely serves as an electron source or sink [5].

In this study a comparison is made between the electrode behaviour of porous gold and platinum electrodes on the $Bi_2Cu_{0.1}V_{0.9}O_{5.35}$ electrolyte (BiCuVOx). In the first part the temperature range between 200° and 500°C is investigated using electrochemical impedance spectroscopy (EIS) and polarization (*I-V*) measurements. These initial results have already been described in the previous two-month report [6]. For completeness these results have been included again in this final report.

New in this report is the study of silver electrodes and the comparison of these with the Pt and Au electrodes in the temperature range between 500° and 735°C. Here also the influence of the partial pressure of oxygen and of applied bias (current carrying conditions) was studied using electrochemical impedance spectroscopy. Also several polarisation experiments have been performed on all three types of electrodes.

2 Experimental procedure

2.1 Material and sample preparation

The BiCuVOx samples (composition $Bi_2Cu_{0.1}V_{0.9}O_{5.35}$) were prepared by the group of Prof. Dunn at UCLA. The samples were sintered individually. The dimensions after sintering were roughly 11.6 mm in diameter and between 2 and 3 mm thick.

As the BiCuVOx material is mechanically rather soft the samples were hand polished on one side. Pt or Au electrodes were sputtered on both sides of the samples. For these electrodes an annular shape was used with an inner diameter of 5.8 mm and an outer diameter of 10.4 mm, resulting in an approximate geometrical surface area of 58 mm^2. The thickness of the Au electrode was estimated at 1.2 µm and the Pt electrode at 0.3 µm. The electrodes were made porous by means of an anneal step at 750°C for two hours in air. Heating and cooling rates were 2°C/minute. The electrode morphology of the electrodes on the polished side of the samples (i.e. the working electrodes) were characterized by SEM.

In the second period of this investigation also silver electrodes were included. In order to improve the electrode properties it was tried to make cermet type electrodes (a sintered, intimate mixture of finely powdered Ag and BiCuVOx). Approximately equal volumes of Ag and BiCuVOx powders were mixed together. In a steel die a sandwich structure was built up by placing a thin layer of the cermet mixture on the bottom, followed by a thick layer of pure BiCuVOx powder and again a thin layer of the cermet mixture. After uniaxial pressing the sample was released from the die and sintered at 750°C in air for two hours, using heating and cooling rates of 2°per minute. Unfortunately this resulted in a totally disintegrated sample, indicating that a reaction between the silver and the BiCuVOx must have taken place (dissolution of the Ag in the BiCuVOx material?). A quick DSC study on the cermet electrode mixture did not show, however, any significant thermal effects up to a temperature of 700°C.

As a second option dense silver layer electrodes were prepared by sputtering (see above) followed by vacuum evaporation of silver using the same electrode geometry as for the Au and Pt electrodes. The layer thickness was not be measured, but it was estimated to be at least 1 µm thick. These electrodes were annealed in situ at a temperature of 710°C for 10 hours before electrochemical measurements were performed.

2.2 Measurement system

Electrochemical measurements were performed in a three-electrode arrangement, see fig. 1, with either all-gold or all-platinum contact measurement cells. The sample with porous gold electrodes was placed in the all-gold contact measurement cell. Annular gauze disks of gold were placed between the contacts and the electrodes in order to provide open space for a free flow of the ambient at the electrodes. As reference electrode a gold point electrode was placed in the centre of the annul of the working electrode, see figure 1. The samples with platinum and with silver electrodes were placed in the all-platinum contacts cell. For both the samples with platinum and with silver electrodes annular gauze disks of platinum were used as spacers in order to provide free flow of the ambient at the electrode area. The annular electrode on the not polished side of the sample (a somewhat rough surface) serves as the counter electrode (current source/sink). The electrodes were connected to a potentiostat (Bank LB75L). For impedance measurements the potentiostat was connected to the frequency response analyser (Solartron FRA 1250).

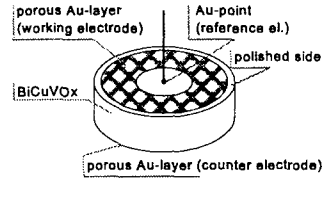

Fig. 1 Schematic representation of the electrode arrangement. A similar annular electrode is placed on the back side. Shown is the sample with gold electrodes.

Impedance measurements were performed as function of temperature, oxygen partial pressure and also at several electrode polarisation levels (bias levels in the range of -0.2 to +0.2 V). These latter two measurement series were only performed at temperatures above 700°C. The oxygen partial pressure was set using two flow controllers for providing a mixture of O_2 and N_2. The exact gas phase composition was not checked at this time. The 'pure nitrogen' does contain still a small amount of oxygen as it was derived from a liquid nitrogen storage tank. It was assumed that the oxygen content of the '100% N_2' gas stream would be smaller than 1%.

Polarisation measurements (*I-V* curves) were measured under computer control using the same potentiostat. The polarisation voltage was incremented in fixed steps of approximately 0.005 V. After a fixed time (typically 2 minutes) the polarisation current was measured and the next voltage increment was applied. This is comparable to a sweep rate of $7.5 \cdot 10^{-5}$ $V \cdot s^{-1}$. When other sweep rates are used this will be indicated.

In the 'low temperature range' (200° to 500°C) the impedance measurements were performed at zero polarisation. In the high temperature range (500° to 735°C) also impedance measurements under polarization (i.e. under current carrying conditions) were performed. All impedance data were analysed with the software package 'Equivalent Circuit' [7,8]. Often the validity of the impedance data was checked with the 'Kramers-Kronig' transform test program [9]. The polarisation curves were handled using a standard spread sheet program.

3 Results

3.1 Characterisation of electrode structure

3.1.1 Gold electrodes

The morphology of the gold electrode, after the annealing experiment, is presented in figure 2. This structure, with small holes in a continuous gold layer, has been found to be typical for thin layer gold electrodes. This structure, however, is not stable during the electrochemical characterisations at high temperatures (735 °C, see below). As not to damage the electrodes no analysis of the electrode structure was made during the electrochemical measurements.

After these measurements were finished the electrodes were re-analysed with a scanning electron microscope (SEM). A representative electron micrograph for the gold electrode is presented in figure 3. From this figure it is clear that significant gold diffusion on the BiCuVOx surface has taken place and recrystallisation of the gold has occurred. An indication of this structural instability was already noticed in the poor reproducibility of the electrochemical measurements.

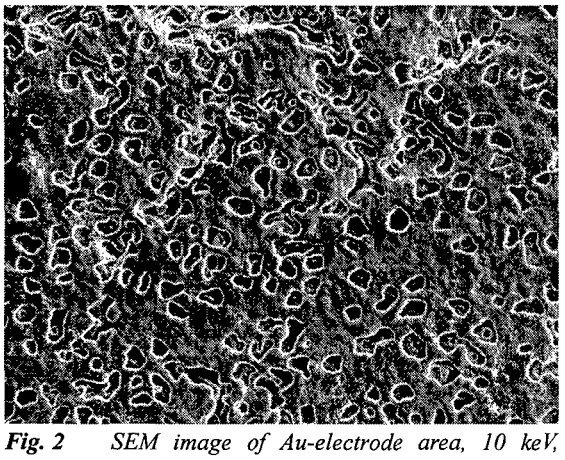

Fig. 2 *SEM image of Au-electrode area, 10 keV, 1000x magnification (orig.).*

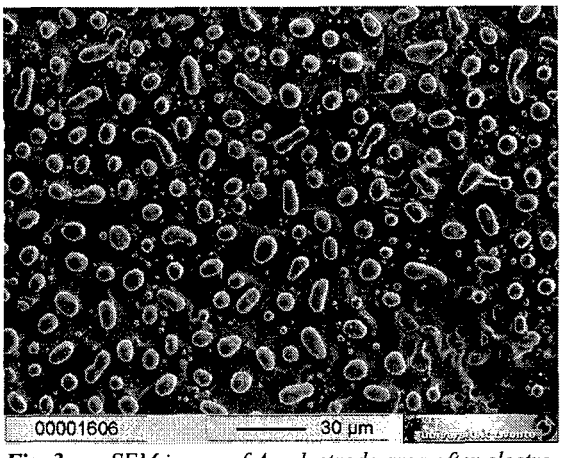

Fig. 3 *SEM image of Au-electrode area after electrochemical experiments. 500x magnification (orig.).*

3.1.2 Platinum electrodes

The morphology of the thin layer platinum electrodes, after the high temperature anneal procedure, is quite different from the gold electrodes. Again the observed structure (see figure 4, next page) is quite typical for Pt on a solid electrolyte. This difference in structural development in thin film electrodes has been seen in previous studies using Pt and Au on yttria stabilized zirconia (YSZ, [10]) and on 25m/o erbia stabilized bismuth oxide (BiEr25, [3-5]). Whereas the gold layer still forms a continuous sheet interspersed with holes, the platinum electrode shows long open areas with interconnected Pt-strips.

In general Pt-electrodes show a quite stable morphology at high temperatures. Inspection with the SEM of the Pt electrode after the high temperature electrochemical measurements showed a significantly changed structure, see figure 5 on the next page. As for the gold electrode, surface diffusion and recrystallisation of Pt must have changed the electrode morphology.

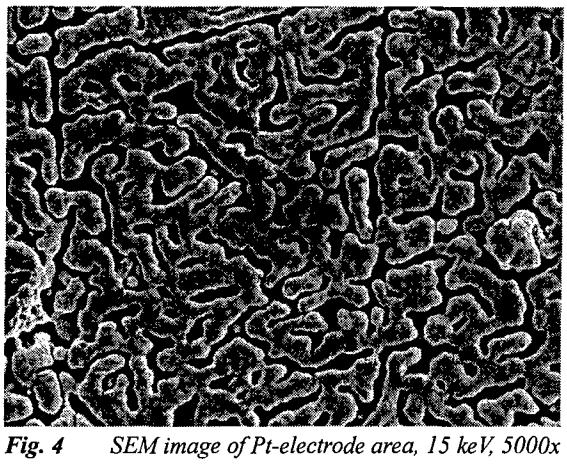

Fig. 4 *SEM image of Pt-electrode area, 15 keV, 5000x magnification (orig.)*

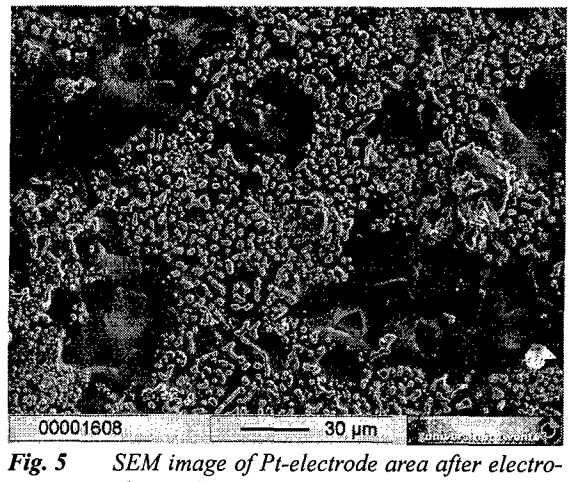

Fig. 5 *SEM image of Pt-electrode area after electrochemical experiments, 500x magnification (orig.)*

3.1.3 Silver electrodes

The silver electrode was not examined with the SEM prior to the electrochemical measurements. From visual inspection a shiny continuous annular shaped silver layer could be observed. After the electrochemical experiments the position of the silver annul could hardly be observed visually. The SEM analysis showed that most of the silver layer had disappeared. Only a few tiny specks were found in the SEM image, as can be seen in figure 6. With respect to the earlier findings of high 'reactivity' of silver towards BiCuVOx, and the original thickness of at least 1µm, it must be concluded that the major part of the silver had dissolved in the BiCuVOx material. Interestingly, still significant electrochemical activity could be measured, as will be shown in the following chapter.

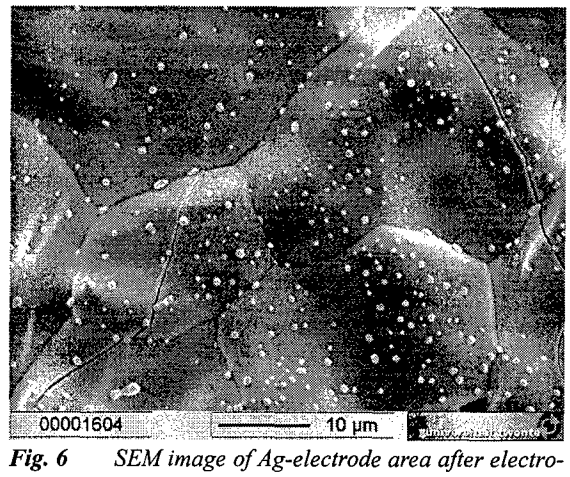

Fig. 6 *SEM image of Ag-electrode area after electrochemical experiments, 2000x magnification (orig.).*

3.1.4 Sample morphology

The samples, which are probably around 90-92% dense (relative to the theoretical density), showed besides small pores also some surface cracks. This can be seen in the surface morphology of the exposed sample area in the centre of the working electrode (polished surface). The SEM micrographs were taken after the anneal step in the preparation of the Au- and Pt-electrodes. Cracks are indicated by the white arrows in figures 7 and 8 on the next page. Whether these cracks were already present in the 'as received' samples has not yet been determined. It is possible that these cracks resulted from the annealing process.

Fig. 7 *SEM image of central area of polished side of Au electrode, 10 keV, 1000x magnification (orig.).*

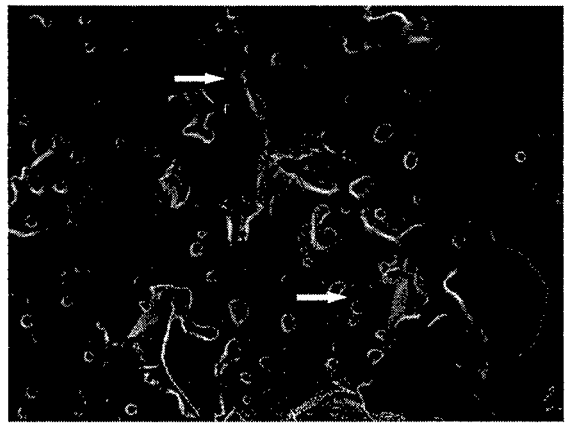

Fig. 8 *SEM image of central area of polished side of Pt electrode, 15 keV, 1000x magnification (orig.)*

3.2 Low temperature measurements (<500°C)

3.2.1 Impedance Measurements (Pt and Au only)

The electrode impedances for both the gold and the platinum electrode show a distinct diffusion behaviour. This Warburg type behaviour is characterized by an almost 45° slope in the frequency dispersion in the impedance plane, see figure 9. CNLS-analysis of the obtained impedance spectra for both electrodes could be based on a common equivalent circuit model ('EqC'), containing two diffusion type elements. The general arrangement of the EqC is presented in figure 10. The notation 'Q' is used for the constant phase element (CPE) which is defined in the admittance representation by:

$$Y_{CPE}(\omega) = Y_0(j\omega)^n = Y_0\omega^n[\cos\frac{n\pi}{2} + j\sin\frac{n\pi}{2}] \quad (1)$$

For n=1 the CPE becomes a pure capacitance (C=Y_0). For n=0.5 a Warburg (diffusion element) is obtained, where Y_0 is related to the (chemical) diffusion coefficient of the mobile species: $Y_0 \div \sqrt{D}$. With n=0 a resistance results (R=Y_0^{-1}).

The double layer capacitance (related to the metal/electrolyte interface) is only noticeable at low temperatures (175 to 250°C). The low frequency electrode resistance, R_4, becomes only apparent above 450°C. Below this temperature it can only be obtained through measurements extended to very low frequencies. The values of the CPE-elements are rather close (within a factor 10) which makes a

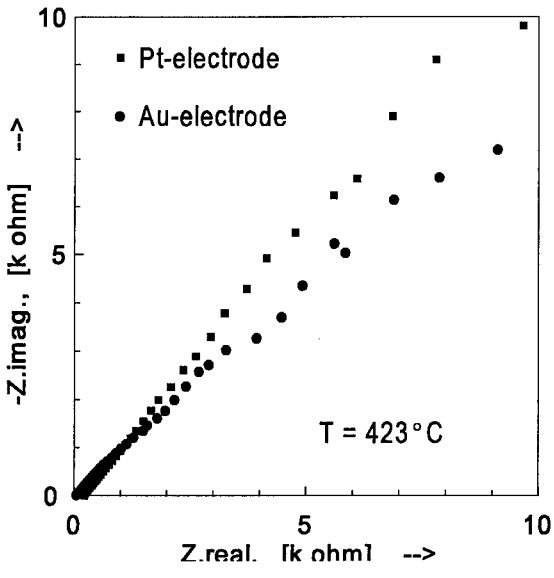

Fig. 9 *Electrode impedances of the Pt (●) and Au (■) electrodes at 423 °C in oxygen.*

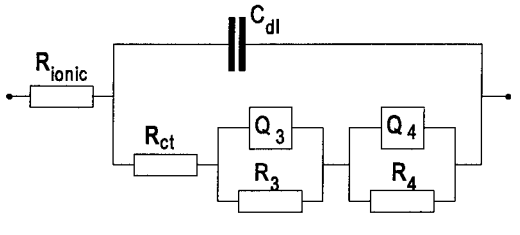

Fig. 10 *General equivalent circuit used in the CNLS-analysis of the electrode impedance measurements.*

reliable analysis impossible. Indications are, however, that the low frequency CPE (Q_4) is less dependent on the electrode type than Q_3 is.

From measurements at 473 °C the *dc*-electrode resistance can be estimated, about 4 kΩ for the gold electrode (see figure 11) and 10 kΩ for the Pt electrode (figure 12). The error margins are, however, quite large. It should be noted that the used EqC not necessarily does represents the actual electrochemical processes in the electrode. Also other EqC's may exist that will model the measured dispersions equally well within the experimental error limits.

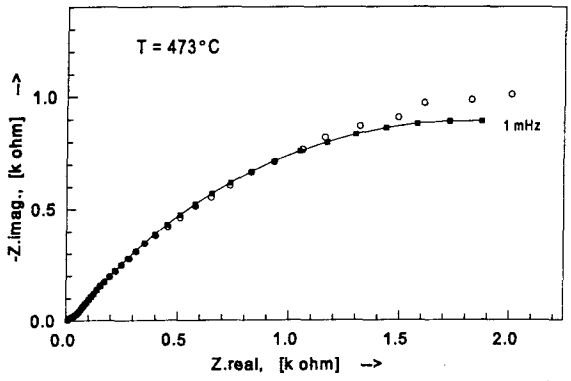

Fig. 11 *Impedance plot for the gold electrode. (O) measurement, (-■-) CNLS-fit.*

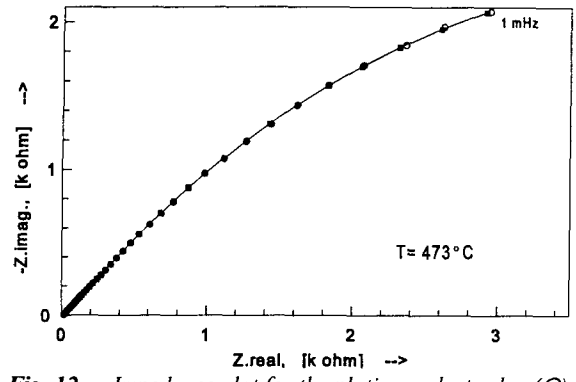

Fig. 12 *Impedance plot for the platinum electrode. (O) measurement, (-■-) CNLS-fit.*

3.2.2 Polarisation measurements

Polarisation measurements were performed at 473 °C. The response showed a significant hysteresis, even at a low scan rate of approximately $7.5 \cdot 10^{-5}$ V·s^{-1}. The polarisation curve and the corresponding Tafel plot for the gold electrode are presented in figures 13 and 14. For the platinum electrode these results are presented in figures 15 and 16 on the next page. These graphs have not been corrected for the ohmic offset, which is due to the bulk resistance of the BiCuVOx electrolyte. Because of the very high ionic conductivity of the BiCuVOx this correction for the non-Faradaic resistance would introduce only a minor change in the *I-V* curves.

In the anodic direction oxygen is evolved from the electrode with the overall reaction given by:

$$2O^{=} \rightarrow O_2 + 4e \qquad (2)$$

while in the cathodic direction oxygen is reduced at the electrode:

$$O_2 + 4e \rightarrow 2O^{=} \qquad (3)$$

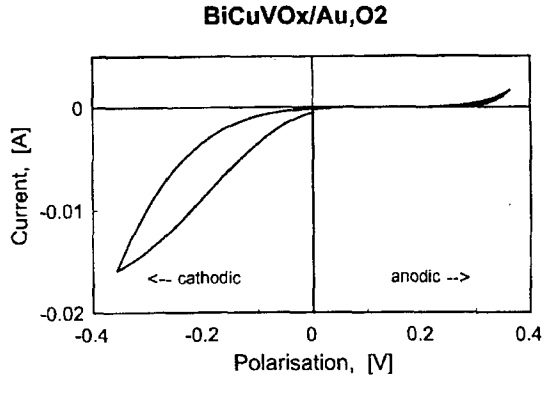

Fig. 13 *Polarisation curve for the gold electrode in oxygen at 473 °C. Plot is not corrected for the non-Faradaic resistance.*

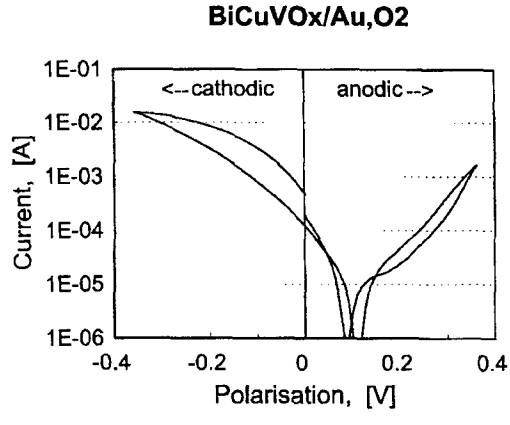

Fig. 14 *Tafel plot of the polarisation curve for the gold electrode, figure 13.*

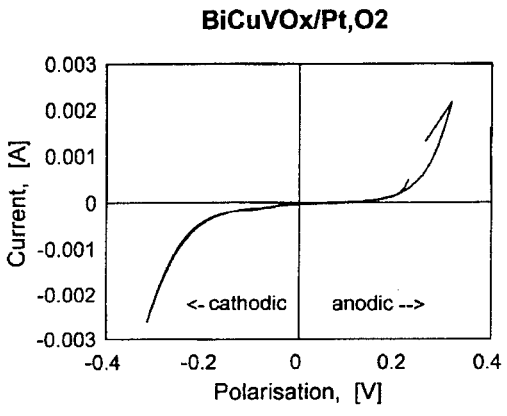

Fig. 15 *Polarisation curve for the platinum electrode in oxygen ar 473 °C. Plot is not corrected for the non-Faradaic resistance.*

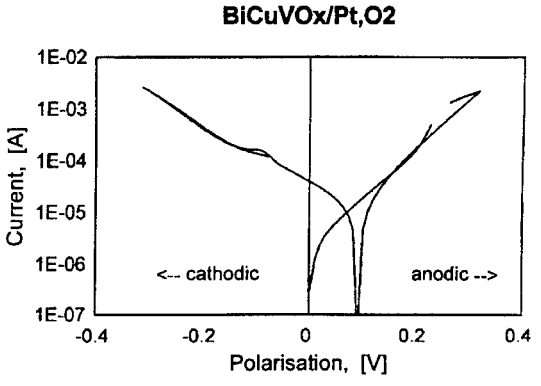

Fig. 16 *Tafel plot of the polarisation curve for the platinum electrode, fig. 15.*

It was found that the shape of the *I-V* curves was very dependent on the electrochemical history of the sample. Due to some problems with the electrochemical set up the gold electrode had been polarised in anodic direction several times before starting the final polarisation measurement, hence the displacement of the 'point of zero current' (i.e. the polarisation level for which the electrode current becomes zero) with respect to the position of zero polarisation.

The influence of the polarisation history on the shape of the *I-V* curve is clearly demonstrated in the (corrected) polarisation curve of figure 17. One complete cycle was recorded starting in the cathodic direction. The direction and sequential order of the polarisation is indicated in the figure.

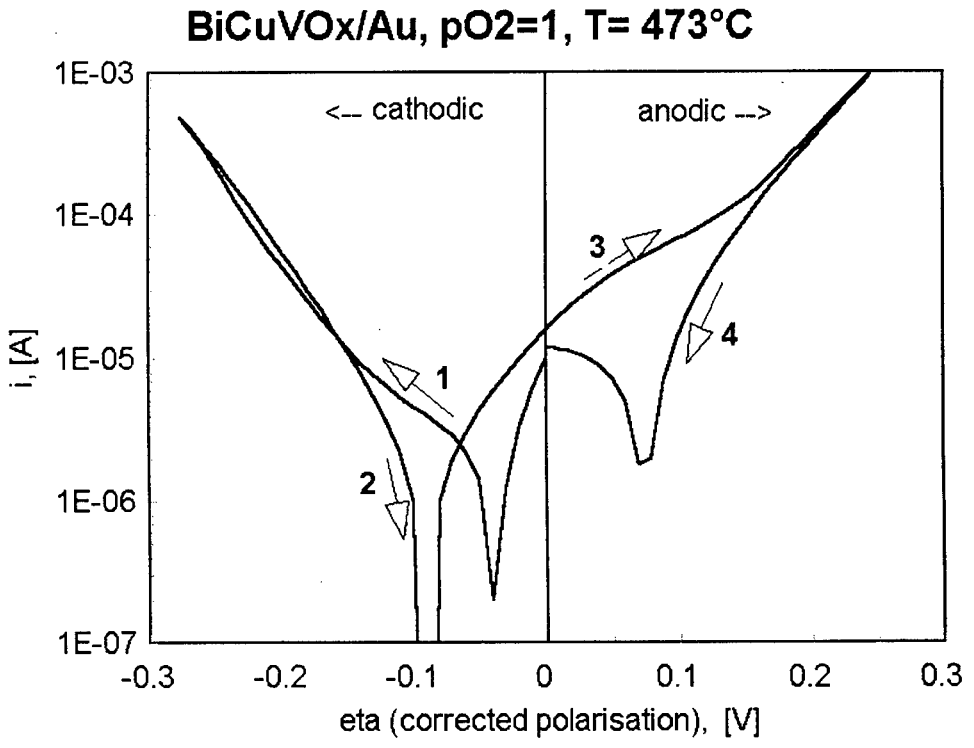

Fig.17 *True polarisation curve for the gold electrode on BiCuVOx at 473 °C and pO_2=1 atm. The sequential polarisation directions are indicated by the numbers and arrows.*

3.3 High temperature measurements (500<*T*<750 °C)

As explained in chapter 3.1, the electrode structures did change considerably with time and temperature. Hence the results presented here can only be seen as emerging trends. Nevertheless some important findings are made. A general picture can be put together for all three different electrodes. The electrode impedance is dominated by a diffusion impedance in the mid-frequency region (1 - 100 Hz). This is a combination of a Warburg-like CPE (n is close to 0.5) parallel to a resistance, $(RQ)_{diff.}$. Upon proper analysis another parallel RQ combination can be discerned at the high frequency side of the impedance spectrum. Its contribution to the overall electrode impedance, however, is rather small. This RQ pair, $(RQ)_{hf.}$ will not be considered here due to the, rather large, uncertainty in the estimation of the parameter values. In the low frequency region (<0.1 Hz) also a (mostly) diffusion type parallel RQ-circuit is seen, but here the power of ω, n, shows more variation between 0.5 (Warburg) and 0.9 (close to capacitive). In the analysis of the most impedances of the gold electrodes clearly a *negative* parallel RC-combination was needed for an optimum fit result. The consistent temperature and pO_2 dependence of this negative pair shows that this combination is a realistic part of the model equivalent circuit.

The overall equivalent circuit is presented in figure 18. Not all elements are observed for all electrodes or measurement conditions. The mid-frequency, $(RQ)_{diff.}$, and the low frequency, $(RQ)_{lf.}$, sub-circuits can clearly be identified for most electrode impedances. The model circuit, presented in figure 18, is only used as a means of data reduction and analysis. It does not necessarily present a physical model for the electrochemical processes at the electrodes.

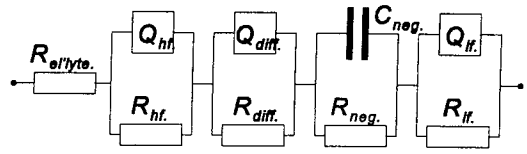

Fig. 18 General equivalent circuit used for analysis of impedance spectra of electrodes above 500 °C.

3.3.1 Impedance of gold electrodes

A typical impedance diagram for the gold electrode is presented in figure 19. The low frequency limit is 3 mHz. The CNLS-fit results, obtained for the model circuit of figure 18 are presented in table 1. Remarkable features are the large values for the negative capacitance (~2 Farad) and for the low frequency CPE (2 $S \cdot s^{-0.75}$). These values are most likely connected to 'chemical' capacitances, e.g. a change in the composition in the surface region of the electrolyte.

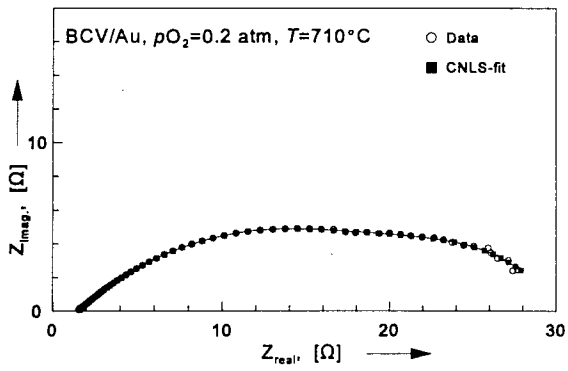

Fig. 19 Impedance of a gold electrode at 710 °C and pO_2=0.2 atm. The instrumental high frequency inductance has been subtracted.

***Table 1** CNLS-fit results for the impedance spectrum of figure 19, a gold electrode at 710 °C and 0.2 atm. oxygen.*

Element		value	error %	unit
$R_{electrolyte}$	:	1.48	0.3	Ω
$R_{hf.}$	:	0.075	0.4	Ω
$Q_{hf.}$, $-Y_0$	:	$8 \cdot 10^{-4}$	15	$S \cdot s^{-n}$
,, $-n$	:	0.97	50	-
$R_{diff.}$	:	24	7	Ω
$Q_{diff.}$, $-Y_0$	:	0.030	2	$S \cdot s^{-n}$
,, $-n$	:	0.48	0.7	-
$R_{neg.}$	:	-0.60	0.4	Ω
$C_{neg.}$, $-Y_0$	:	-2.0	20	F
$R_{lf.}$	:	5.0	23	Ω
$Q_{lf.}$, $-Y_0$	:	2.1	15	$S \cdot s^{-n}$
,, $-n$	:	0.75	30	-

3.3.1.1 Influence of the oxygen partial pressure on the electrode impedance

The dependence of the electrode impedance on the pO_2 was measured at 710 °C under the following O_2/N_2 gas flow mixtures: 100% O_2 (1 atm), 50% O_2, 20% O_2, 5% O_2 and 100% N_2. For this last ambient the oxygen partial pressure was estimated to be smaller than 1% (<0.01 atm). In the following diagrams versus pO_2 the results for '100% N_2' are presented at pO_2=0.01 atm. Although this choice seems to fit reasonably well with the data points at higher pO_2, it cannot be used to obtain reliable pO_2 dependence. The overall electrode resistance (apparent dc-value, presented in figure 21 as R_{sum}) does not change much with pO_2. In figure 21 the resistance values are plotted against the pO_2. R_{bcv} represents the electrolyte resistance, which should be independent of pO_2, the high frequency resistance (see the circuit model of figure 18) R_{hf} has not been drawn as its contribution to the overall impedance is very small. The error in the negative resistance, $R_{neg.}$, is rather large. Drawn lines are only used to connect same parameter values.

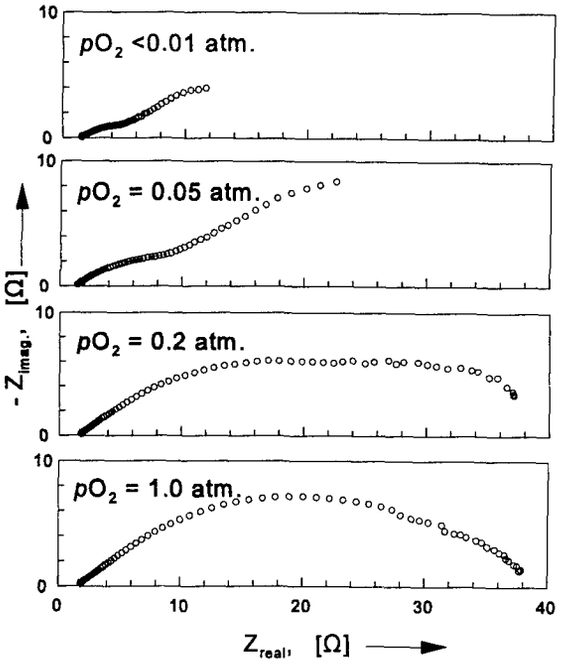

Fig. 20 Electrode impedance of BCV/Au system at 710 °C as function of pO_2.

The constituents, however, do show marked dependence on pO_2, as can also be observed from the change in the impedance with pO_2, figure 20. Despite the high temperature, the samples need considerable time to equilibrate after a change of the PO_2. As this conditions is not always met this can result in considerable scatter in the data.

The major part of the electrode resistance is attributed to $R_{diff.}$ The main dispersion is also caused by the CPE in parallel to $R_{diff.}$, which is almost a Warburg type diffusion element. It is important to note that $R_{diff.}$ *decreases* with decreasing pO_2, while at the same time the Y_0-value of $Q_{diff.}$ *increases*. This implies that, with respect to $(RQ)_{diff.}$, the electrode performance *improves* with decreasing pO_2, which is quite an unusual result. The double log plot, figure 22, seems to suggest a $(pO_2)^{\pm 1/2}$ behaviour for these two elements.

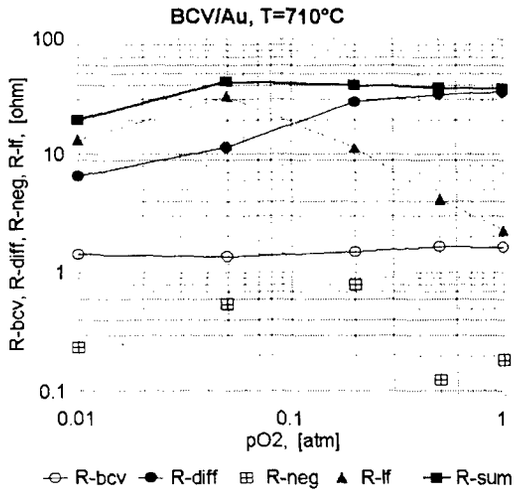

Fig. 21 pO_2 dependence of the resistances for the gold electrode, as obtained from the CNLS-fit procedure using the model of fig. 16.

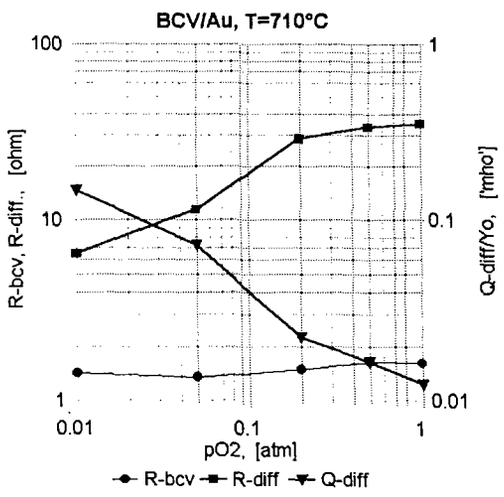

Fig. 22 pO_2 dependence of the major diffusion element parameters. The electrolyte resistance is presented for comparison.

3.3.1.2 *Influence of the polarization on the electrode impedance*

In general all the impedances for the gold electrode could be analysed with the model circuit of figure 18. The high frequency contribution was very small and could not be established with an acceptable accuracy, hence it was not included in the analysis. The measurement results were found to be rather 'history' dependent. Also the wait time after the stepwise change of the polarisation level was not long enough (as could be noted from the Kramers-Kronig validation tests). As a result the polarisation dependence of most circuit parameters showed a rather large scatter. An overview of the polarisation dependence of the electrode dispersion is presented in appendix A.

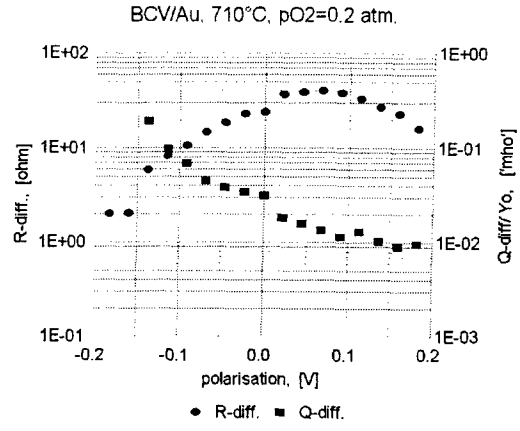

Fig. 23 *Polarisation dependence of the major dispersion elements, $R_{diff.}$ and $Q_{diff.}$ for the Au-electrode.*

Fortunately it was possible to partially analyse the data, based on the major contribution to the overall dispersion, $(RQ)_{diff.}$ The polarisation dependence of the parameters is presented in figure 23. The $R_{diff.}$ shows typical behaviour for a charge transfer resistance. On the anodic side the slope of the curve is close to F/RT. The Y_0 value of $Q_{diff.}$ is also polarisation dependent, indicating an increased diffusion rate for more anodic directions. The important conclusion here is that this diffusion element is closely coupled to the polarisation level and hence to the electron concentration at the interface.

3.3.1.3 *Temperature dependence of the electrode impedance*

After the electrode performance had been measured at the highest temperature (735 °C), the temperature dependence of the electrode impedance was measured at an oxygen partial pressure of 0.2 atm. Again the general circuit model of figure 18 could be applied. As was done above, the high frequency contribution was not included in the analysis. In figure 24 the temperature dependence of the parameter values of the resistances are presented. Although the estimated error in the negative resistance, $R_{neg.}$ was rather large still a consistent result is obtained. R_{bvc} represents the 'uncompensated' electrolyte or 'non-Faradaic' resistance. It is important to note that (for pO_2=0.2 atm.) $R_{neg.}$ remains smaller than R_{bvc} over the entire temperature range. It is also evident that the overall electrode resistance is mainly attributed to $R_{diff.}$.

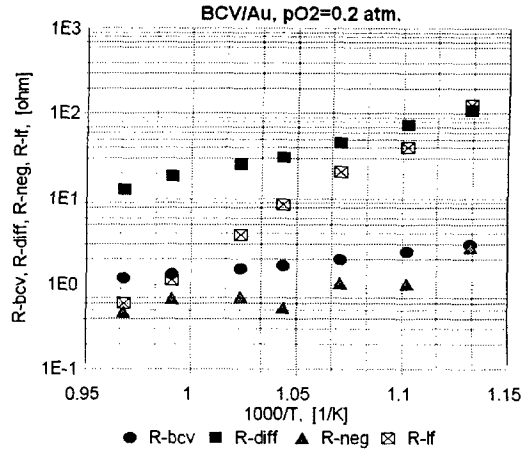

Fig. 24 *Temperature dependence of the resistances of the gold electrode, according to the circuit model of fig. 18.*

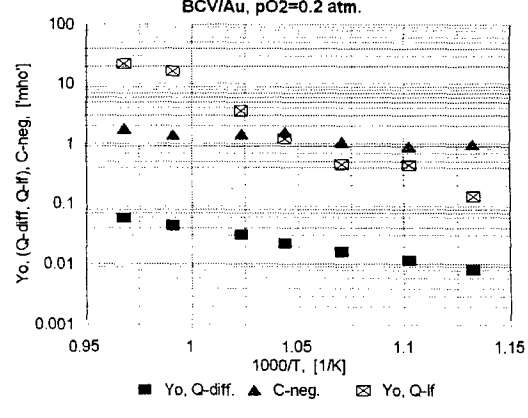

Fig. 25 *Temperature dependence of the Y_0 values of the dispesive elements (CPE's) for the gold electrode, according to the circuit model of fig. 18.*

In figure 25 the temperature dependence of the Y_0 values of the dispersive elements (CPE's) are presented. They all show Arrhenius type behaviour. The associated activation energies for both R and Y_0 values are presented in table 2 (next page).

The frequency 'order' of the CPE's (the parameter n in equation 1) can be used as indication for the underlying physical process. The largest contribution to the dispersion is presented by $(EQ)_{diff.}$. The n-value of this CPE (Q) is close to 0.5, indicating that diffu-

sion of charged species is involved. The negative contribution can best be described with capacitive behaviour ($n = 1$). Because of the difficulty to establish the power of ω for this sub-circuit, it was kept fixed at 1. The n-value for the low frequency contributions showed much more scattered values between 0.3 and 1, although 0.7 to 0.8 was mostly observed. The scatter is most likely due to the rapidly decreasing quality of the data with decreasing frequencies (below about 1 Hz). In this low frequency range the response becomes increasingly sensitive to non-linear effects (due to a too large excitation signal) and external electromagnetic interference, as indicated by the results of the Kramers-Kronig transform tests.

It is interesting to note that for the negative (RC) contribution the activation energies for $R_{neg.}$ and $C_{neg.}$ are equal well within experimental error and also close to the observed $E_{act.}$ for $R_{electrolyte}$. Identical activation energies are also observed for the low frequency contribution, $(RQ)_{low\text{-}f.}$. These activation energies are, however, quite large.

Table 2 *Estimated activation energies for the different sub-circuit parameters of the BiCuVOx/Au, 'air' electrode (at zero polarisation). Results of CNLS-fit (see figures 24 and 25) based on the circuit model of figure 18. Due to its minor contribution the high frequency (RQ) circuit has been omitted.*

Element/	activation energies of sub-circuit elements [kJ·mol^{-1}]:			
parameter:	$R_{electrolyte}$	(RQ)-diffusion	(RC)-negative	(RQ)-low f
Resistance, R	38	107	38	280
CPE, Y_0	--	56	36	300

3.3.2 Impedance of platinum electrodes

The electrode resistance of the porous Pt electrode is consistently higher than the electrode resistance of the Au electrode. This behaviour was already observed from the impedance measurements in the low temperature range (see chapter 3.2). It becomes again evident from the comparison of the pO_2 dependence of the Pt-electrode impedance (figure 26) with the electrode impedance of the gold electrode (figure 20, p.12). For the Pt-electrode the frequency dispersion is again clearly dominated by a diffusion type process, presented by the $(RQ)_{diff.}$ sub-circuit, see the model of figure 18. The power dependence of the frequency, n, for this sub-circuit is very close to 0.5.

As observed for the gold electrodes, a negative (RC) contribution can be detected through a thorough analysis of the impedance data. The *low frequency*, $(RQ)_{lf.}$, sub-circuit, however, is less pronounced (compared to the Au-electrode) and only noticeable at low pO_2's (see figure 26). The high frequency circuit, which gave a minor contribution for the gold electrode, could hardly be observed for the Pt electrode.

The results of a CNLS-analysis of the Pt-electrode response at 710°C and pO_2=0.2 atm. is presented in

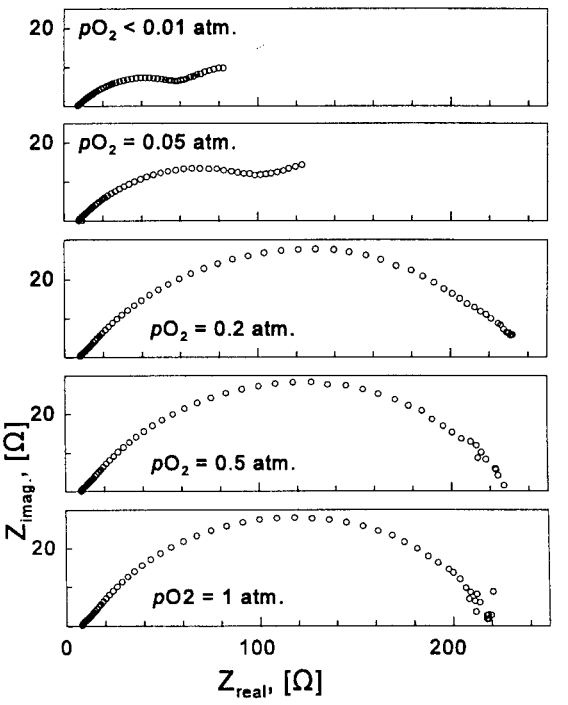

Fig. 26 *Electrode impedance of the BiCuVOx/Pt,O_2 electrode at 710 °C as function of pO_2. Frequency range is 1mHz to 65 kHz.*

Table 3 *CNLS-fit results for the impedance spectrum of figure 26, a platinum electrode at 710 °C and 0.2 atm. oxygen.*

Element		value	error %	unit
$R_{electrolyte}$	:	3.7	0.2	Ω
$R_{hf.}$	:	0.18	6	Ω
$Q_{hf.}$, $-Y_0$	:	0.0006	8	F
,, $-n$	:	1.0	<fixed>	-
$R_{diff.}$	:	124	0.8	Ω
$Q_{diff.}$, $-Y_0$	:	0.0063	0.3	$S \cdot s^{-n}$
,, $-n$	:	0.54	0.5	-
$R_{neg.}$	:	-4.7	11	Ω
$C_{neg.}$, $-Y_0$	:	-1.2	12	F
$R_{lf.}$	:	*n.d.*	-	Ω
$Q_{lf.}$, $-Y_0$	:	*n.d.*	-	$S \cdot s^{-n}$
,, $-n$	:	*n.d.*	-	-

n.d. *= not detected or not accepted by CNLS-fit*

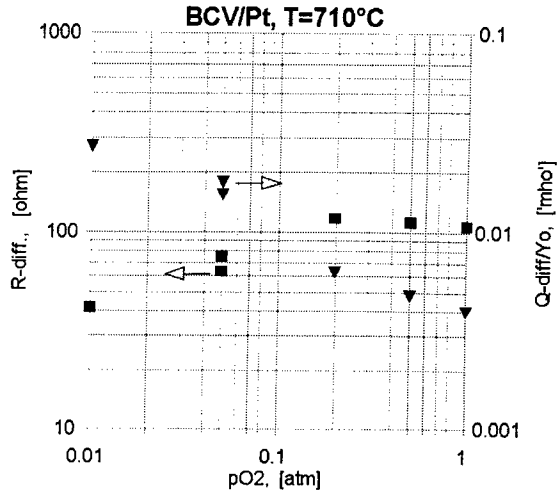

Fig. 27 *pO_2 dependence of the diffusion sub-circuit elements for the Pt-electrode, (■) $R_{diff.}$, (▾) $Q_{diff.}$ (Y_0-value).*

table 3. Comparison with the CNLS-fit results for the Au-electrode under identical conditions (see table 1) shows that $R_{diff.}$ is about a factor 5 larger for the Pt-electrode than for the Au-electrode. Also the Y_0-value for the diffusion CPE ($Q_{diff.}$) is a factor 5 *smaller* than found for the gold electrode. Hence it follows that the 'time constant' (see Appendix B), associated with the diffusion process, $R_{diff.} \cdot Y_{0,\,diff.}$, is virtually independent of electrode type for the same pO_2. Again it can be observed that the diffusion rate *increases* with *decreasing* pO_2, see figure 27. From this figure a $Y_0 \div pO_2^{-½}$ can be inferred as was also noticed for the Au-electrode. The associated resistance, $R_{diff.}$, shows a maximum at about 0.2 atm. O_2, which is in contrast with the results obtained for the gold-electrode (figure 22).

In the high temperature range no temperature dependence of the Pt-electrode impedance was measured. Preliminary electrode impedance measurements for different polarisation levels show in principle the same behaviour as observed for the gold electrode.

3.3.3 Impedance of silver electrodes

In chapter 3.1.3 it was indicated that the silver electrodes possibly had reacted with the BiCuVOx electrolyte. This observation was done *after* the electrochemical experiments were concluded. It was observed that the general pattern of behaviour of the Ag-electrode closely resembled those of the Au- and the Pt-electrode. Hence it is still useful to include the findings for the Ag-electrode in this report. One should be aware, however, that the electrode/electrolyte interface may have quite different properties with respect to those of the Au- and Pt-electrodes.

One remarkable difference is that the negative (RC) circuit in the low frequency region could not be detected with accuracy. Due to the noise in the low frequency region of the spectrum and the distortions due to non linear behaviour this circuit could not be included in the CNLS-analysis. An example of a CNLS-fit is presented in Table 4. As the 'diffusion' type sub-circuit, $(RQ)_{diff.}$, again presents the largest contribution to the overall frequency dispersion of the electrode, only the $R_{diff.}$ and $Q_{diff.}$-Y_0 parameters will be considered in the analysis.

Table 4 *CNLS-fit results for the impedance spectrum of a silver electrode at 705 °C and 0.2 atm. oxygen.*

Element		value	error %	unit
$R_{electrolyte}$	:	1.44	0.2	Ω
$R_{hf.}$	:	1.8	20	Ω
$Q_{hf.}$, $-Y_0$	:	0.06	6	$S \cdot s^{-n}$
,, $-n$	:	0.82	4	-
$R_{diff.}$	:	57.7	0.7	Ω
$Q_{diff.}$, $-Y_0$	:	0.014	1.6	$S \cdot s^{-n}$
,, $-n$	:	0.576	0.2	-
$R_{neg.}$	:	*n.d.*	-	
$C_{neg.}$, $-Y_0$	:	*n.d.*	-	
$R_{lf.}$	:	3.3	8	Ω
$Q_{lf.}$, $-Y_0$	:	17	10	F
,, $-n$	:	1	<fixed>	-

n.d. *= not detected or not accepted by CNLS-fit*

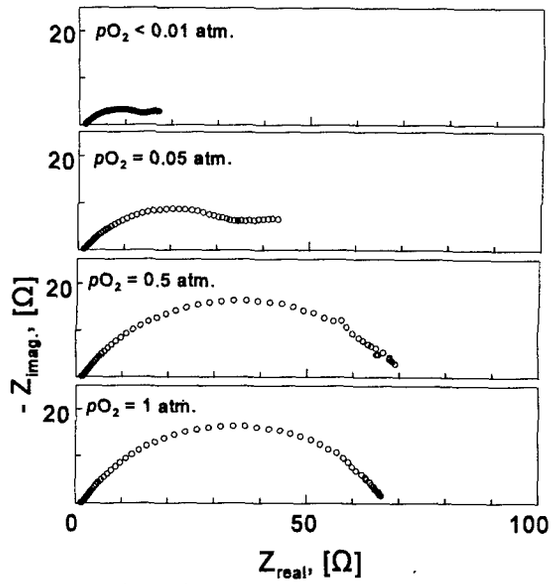

Fig. 28 *Electrode impedance of the BiCuVOx/Ag,O_2 electrode at 700 °C as function of pO_2. Frequency range is 1 mHz to 65 kHz.*

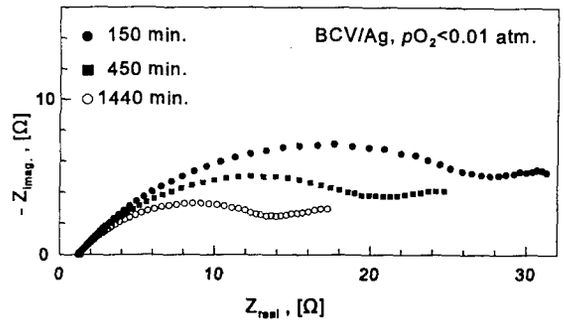

Fig. 29 *Change of the electrode impedance with time after a step in the pO_2 from 0.05 atm to <0.01 atm. BiCuVOx/Ag electrode system.*

3.3.3.1 *Influence of the oxygen partial pressure on the electrode impedance*

In figure 28 the change in shape of the impedance is presented as function of the pO_2. The electrode was found to respond rather slowly to a step change in the pO_2. This is clearly indicated by the change in the shape of the impedance with time upon a step change in the oxygen partial pressure from 0.05 atm. to less than 0.01 atm., see figure 29. It is noteworthy that the 'time constant', $\tau_{diff.} = R_{diff.} \cdot Y_{0,diff.}$, associated with the $(RQ)_{diff.}$ sub-circuit, remains virtually constant during the change with time, see Table 5.

In figure 30 (next page) the pO_2 dependencies of $R_{diff.}$ and $Y_{0,diff.}$ are presented. The contribution to the overall impedance of the low frequency (RQ) circuit quickly diminishes with increasing pO_2. Because of the rather large scatter in the estimated parameter values of this sub-circuit these are not considered further in the data analysis procedure.

Also for the Ag-electrode the diffusion type $(RQ)_{diff.}$ sub-circuit presents the most pronounced contribution to the electrode impedance. In contrast to the results for the Au- and Pt-electrodes (figures 22 and 27), figure 30 seems to indicate a $pO_2^{-1/4}$ dependence for $Y_{0,diff.}$. The resistance, $R_{diff.}$, on the other hand, shows a maximum around $0.2 < pO_2 < 0.5$ atm., somewhat higher than observed for the Pt-electrode.

Table 5 *Variation of the diffusion time constant, $\tau_{diff.}$, with time after step in the pO_2 ambient (see figure 29).*

time (min.)	$R_{diff.}$ [Ω]	$Q_{diff.}$, Y_0 [$S \cdot s^{-n}$]	'$\tau_{diff.}$'
150	31	0.031	0.95
450	22.3	0.044	0.98
1440	14.6	0.069	1.01

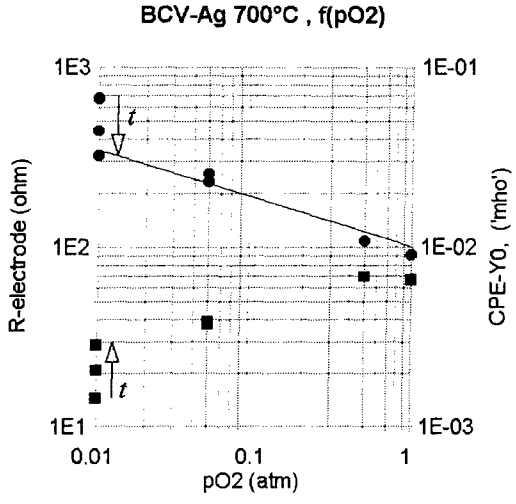

Fig. 30 *pO_2 dependence of the parameters, $R_{diff.}$ (■) and $Y_{0,\,diff.}$ (●) of the diffusion sub-circuit for the Ag-electrode. Arrows indicate direction of change with time after a step change in the pO_2. Temperature is 705 °C.*

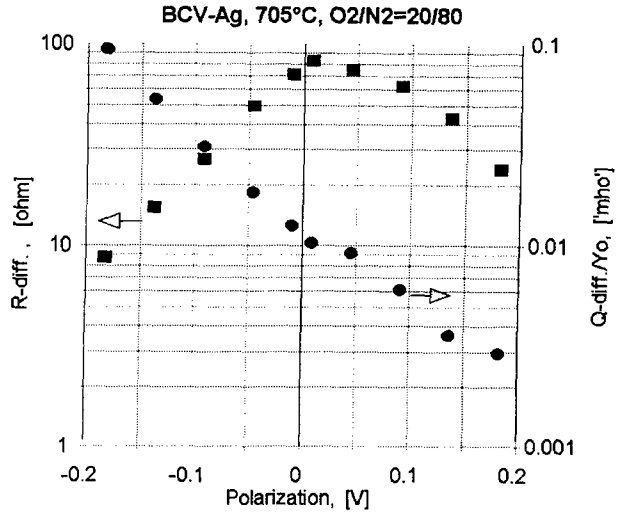

Fig. 31 *Polarisation dependence of the parameters, $R_{diff.}$ (■) and $Y_{0,\,diff.}$ (●) of the diffusion sub-circuit for the Ag-electrode. Measurement at 705 °C and pO_2 = 0.2 atm..*

3.3.3.2 *Influence of the polarization on the electrode impedance*

The polarisation dependence of the $(RQ)_{diff.}$ parameters, $R_{diff.}$ and $Y_{0,\,diff.}$ are presented in figure 31. These results are quite identical to those for the polarisation dependence of the Au-electrode (figure 23). The resistance, $R_{diff.}$, shows typical 'charge transfer' characteristics, although the maximum in $R_{diff.}$ does not coincide exactly with the polarisation level η=0. The slope on the cathodic side corresponds quite well with F/RT. The slope of Y_0 of the diffusion CPE shows almost a $-F/RT$ slope indicating that the diffusion is also directly connected to the polarisation level: $Y_0 \div \exp(-F\eta/RT)$.

3.3.3.3 *Temperature dependence of the electrode impedance*

For the temperature dependence of the BiCuVOx/ Ag-electrode system only accurate parameter values could be obtained for the diffusion type sub-circuit. In figure 32 an Arrhenius plot of the $R_{diff.}$ and the $Y_{0,\,diff.}$ parameters are presented. The estimated activation energies are about 120 kJ·mol^{-1} for $R_{diff.}$ and 75 kJ·mol^{-1} for $Y_{0,\,diff.}$, somewhat higher than found for the Au-electrode (107 resp. 56 kJ·mol^{-1}, see table 2).

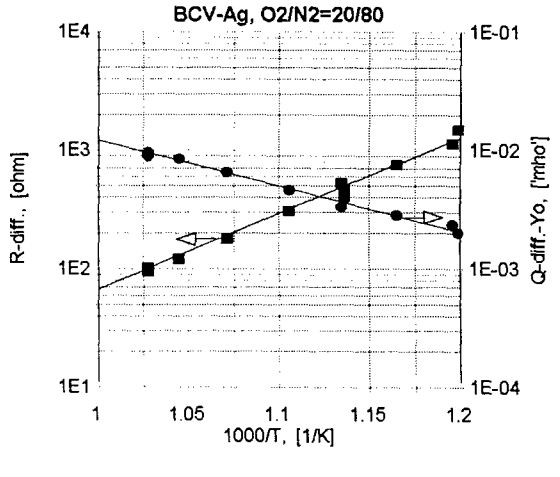

Fig. 32 *Temperature dependence of the parameters of the diffusion sub-circuit, $(RQ)_{diff.}$: (■) $R_{diff.}$,(●) $Y_{0,\,diff.}$. Ag-electrode in 0.2 atm. oxygen.*

3.3.4 Polarisation measurements

Polarisation measurements (*I-V* curves) were performed at the highest test temperature, 735 °C. The ambient was a 80% N_2 / 20% O_2 gas mixture at 1 atm., indicated by 'air'. The polarisation voltage of the working electrode, imposed by a potentiostat, was changed in a stepwise fasion. In general the voltage was incremented (or decremented) in 5 mV steps. The cell current was then measured 60 s after the step change and was followed by the next step change. This results in an effective sweep rate of 83 $\mu V \cdot s^{-1}$, or an equivalent large signal 'sweepfrequency' of 68 μHz.

3.3.4.1 I-V characteristics of the gold electrode

Figure 33 presents the polarisation curve for the BiCuVOx/Au-electrodes in the form of a 'Tafel-plot'. In principle the polarisation voltage should be corrected for the 'non-Faradaic' contribution, of the electrolyte resistance, $R_{electrolyte}$, thus yielding the actual electrode polarisation, η:

$$\eta = V_{appl.} - I_{electrode} \cdot R_{electrolyte} \qquad (4)$$

It was observed, however, that $R_{electrolyte}$ is not a constant but depends on the electrode current. At small polarisation levels this correction is rather small, thus it is allowed to make an estimate of the exchange current of the electrode. The error introduced by excluding the correction can be seen in the decrease of the log(*I*) vs *V* slope (Tafel slope) at the highest polarisation levels. On the other hand, applying the correction of eq. (4), by using the $R_{electrolyte}$ value obtained *at V*=0, will lead to an unrealistic increase of the slope in the higher polarisation regions.

At a higher scan rate of 2 $mV \cdot s^{-1}$ again a distinct hysteresis in the location of the 'zero current' polarisation level is observed, see figure 34, though the deviation from V (or η) = 0 is smaller than observed at lower temperatures (see figure 17). At a lower scan rate (25 $\mu V \cdot s^{-1}$) virtually the same curve is obtained as presented in figure 33.

3.3.4.1 I-V characteristics of the platinum electrode

The Tafel plot for the BiCuVOx/Pt-electrode is presented in figure 35. The scan rate was 83 $\mu V \cdot s^{-1}$. Here a distinct hysteresis is observed in the anodic branch, its cause is unclear at present. The response of the Pt-electrode is about a factor 2 smaller than for the gold electrode. Possibly this can be attributed to the development of a less favourable electrode geome-

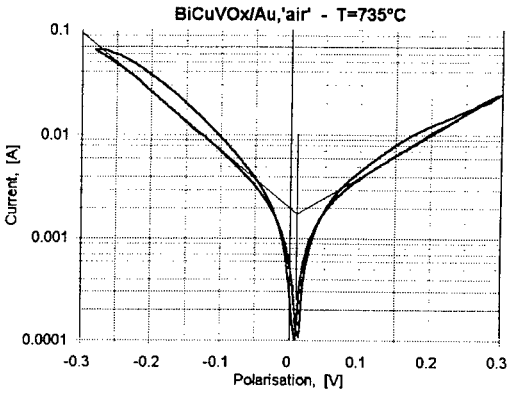

Fig. 33 *Tafel plot for the BiCuVOx/Au,air electrode at 735 °C. The scan rate is 83 $\mu V \cdot s^{-1}$. The polarisation has not been corrected for the 'non-Faradaic resistance'. The drawn lines give an indication of the exchange current, I_0.*

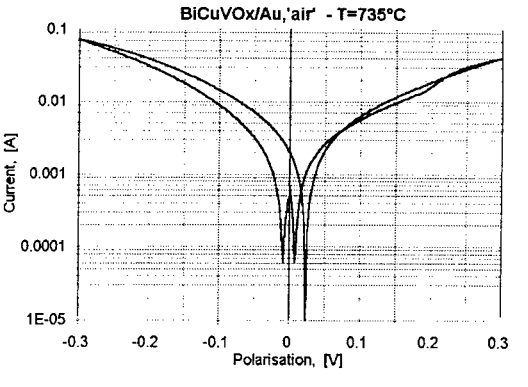

Fig. 34 *Tafel plot for the BiCuVOx/Au,air electrode at 735 °C. Scan rate is 2 $mV \cdot s^{-1}$. Polarisation has not been corrected for the 'non-Faradaic resistance'.*

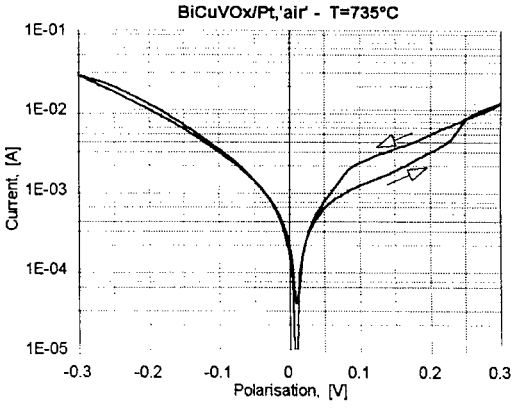

Fig. 35 *Tafel plot for the BiCuVOx/Pt,air electrode at 735 °C. Scan rate is 83 $\mu V \cdot s^{-1}$. Polarisation has not been corrected for the 'non-Faradaic resistance'.*

Table 6 *Summary of the exchange currents (I_0) and exchange current densities (J_0) for the three electrode types measured at 735 °C and in 'air'. Results are estimates from graphical analysis, estimated range is presented by 'low' and 'high'.*

electrode/ scan speed [$\mu V \cdot s^{-1}$]		I_0, [10^{-3} A]		J_0, [$A \cdot m^{-2}$]	
		low	high	low	high
Au,	25	1.6	2.2	28	38
Au,	83	1.8	2.0	31	34
Au,	$2 \cdot 10^3$	2.0	3.0	34	52
Pt,	83	0.5	0.9	8.6	16
Ag,	50	0.3	0.5	4.5	8.6

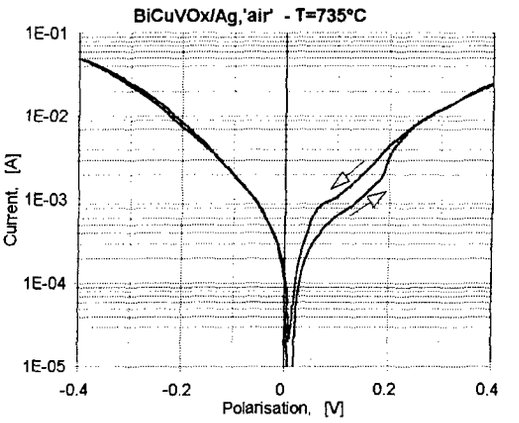

Fig. 36 *Tafel plot for the BiCuVOx/Ag,air electrode at 735 °C. Scan rate is 50 $\mu V \cdot s^{-1}$. Polarisation has not been corrected for the 'non-Faradaic resistance'.*

try due to the continuous 'annealing process' during the measurements at high temperatures (see chapter 3.1.2).

3.3.4.1 I-V characteristics of the silver electrode

A similar hysteresis, as found for the Pt-electrode, is observed for the BiCuVOx/Ag electrode system, see figure 36. The scan rate for this electrode was 50 $\mu V \cdot s^{-1}$. Again the electrode response is smaller than for the Au-electrode, but also smaller than found for the Pt-electrode.

Exchange currents and exchange current densities (based on the geometrical electrode area of 58 mm^2) are presented in Table 6 for the three differen type of electrodes. The values were obtained by simple graphimetrical extrapolation of the Tafel regions, see e.g. figure 33. Both lower- and an upper limit estimates are presented.

4 Discussion

4.1 Electrode response at low temperatures (<500°C)

At moderate temperatures (200° to 500°C) the electrode response is rather small. The general shape of the *ac*-response is the same for the Au and the Pt electrode. Taking into account the strong dependence of the *I-V* curve on the electrochemical history, the most plausible conclusion is that the electrode response is mostly due to changes in the bulk, rather than actual electrode behaviour. It is most likely that, by imposing on the sample a different oxygen activity at the metal-electrode/electrolyte interface, the oxygen stoichiometry of the sample changes by a slow diffusion process. As the oxygen mobility (conductivity) is very high, this diffusion process is controlled by the 'minority charge carriers', i.e. electrons or electron-holes.

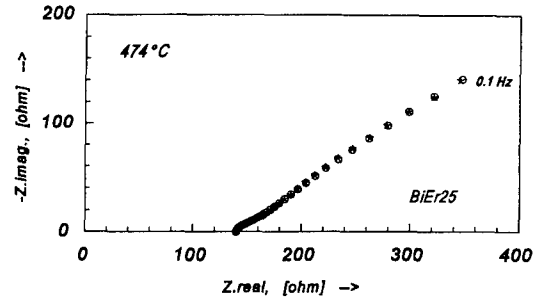

Fig. 37 *Impedance plot for BiEr25/Au,air.*

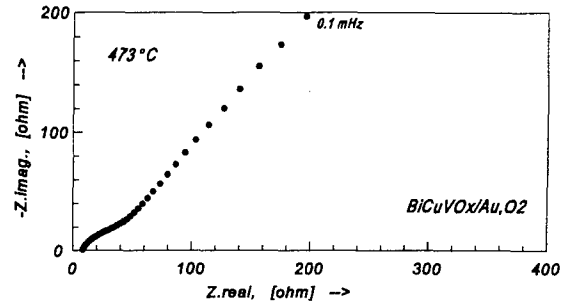

Fig. 38 *Impedance plot for BiCuVOx/Au,O_2.*

This idea is supported by the characteristics of the *I-V* curves. The gold electrode had been polarized anodically for some period of time before the final polarisation curve was measured (see figures 13 and 14). Hence the oxygen concentration in the sample in the electrode/electrolyte interface region had increased with respect to the equilibrium concentration, i.e. a higher oxygen activity results. This is reflected by the shift in the zero-current crossing towards a more anodic polarisation level (figure 14). In the return path from the maximum anodic polarisation, this zero-crossing point has shifted further cathodically, as is to be expected according to the suggested model. An even clearer picture is presented in figure 17, where three different 'zero current' crossings can be observed.

The *ac*-response, however, is quite comparable to the impedance measured for a sputtered gold electrode on erbia doped bismuth oxide, $(Bi_2O_3)_{0.75}(Er_2O_3)_{0.25}$ or abbreviated BiEr25 [3-5]. The impedance measured at 474°C is presented in figure 37. For comparison the impedance of the gold electrode for the same frequency range (0.1 Hz to 10 kHz) is presented in figure 38. In these figures the much higher oxygen ion conductivity for BiCuVOx is quite obvious. The main difference between BiEr25/Au and BiCuVOx/Au is that for the BiEr25 sample a much smaller hysteresis is observed in the *I-V* curves than for the BiCuVOx sample. This may be related to a relatively smaller electronic conductivity for BiEr25.

4.2.1 High temperature impedance response

The high temperature electrode responses measured at zero bias (no polarisation) are quite complicated. In most instances the model circuit of figure 18 could be used for interpretation. Although there are some differences between the different electrode metals, all impedance diagrams show basically the same behaviour. Most prominent is the diffusion type $(RQ)_{diff.}$ sub-circuit, which dominates the impedance spectra. But more remarkable is its pO_2 dependence and its dependence on polarisation level.

With *decreasing* pO_2 the resistance, $R_{diff.}$, also *decreases* while the Y_0-value of the diffusion element ($Q_{diff.}$, a CPE with $\sim 0.45 > n > \sim 0.6$) increases. This indicates that the diffusion rate *increases* with decreasing pO_2. It may safely be assumed that some kind of (charged-) oxygen species is involved in the diffusion process. The oxygen concentration or the oxygen vacancy concentration of the BiCuVOx bulk

will not significantly change as function of pO_2, hence a different mechanism must be responsible for the observed pO_2 dependence of this diffusion sub-circuit.

The same picture holds for the polarisation dependence of $(RQ)_{diff.}$ when it is recognized that negative (cathodic) polarisation amounts to an effective decrease in the oxygen activity (or in the equivalent oxygen partial pressure) in the electrode/electrolyte region. For the silver electrode a very clear exponential relation between the polarisation (η) and the magnitude of the diffusion element, Y_0, is found:

$$Y_0 \div e^{-\frac{F}{RT}\eta} \tag{5}$$

where the slope is equal to F/RT within the experimental error limits, see figure 31. The resistance, $R_{diff.}$, shows the typical polarisation dependence of a charge transfer resistance, with a cathodic charge transfer coefficient of 1. The same behaviour is observed for the gold electrode, although the accuracy in determining the η-dependencies is much lower (figure 23).

On the assumption that the oxygen- and the oxygen vacancy concentration in the BiCuVOx bulk are virtually independent of pO2, the following relation between the electron concentration and the oxygen partial pressure can be derived:

$$O_{2,g} + 4e' + 2V_O^{\cdot\cdot} \rightleftharpoons 2O_O^{x} \quad \text{, hence:} \quad [e'] \div (pO_2)^{-1/4} \tag{6}$$

This can be taken as a clear indication that bulk electrons of the BiCuVOx are directly involved in the diffusion process. The data obtained in this preliminary investigation does not allow, however, to start a detailed analysis of the observed pO_2-dependencies for the different circuit elements.

Another remarkable observation is that, under nearly identical conditions, for the three different electrode types rather different values for $R_{diff.}$ and for Y_0 are found (see Tables 1, 3 and 4) but the associated 'time constants', $\tau_{diff.} = R_{diff.} \cdot Y_0$, are very close (0.7 to 0.8, see Table 7). The time constant is put between quotation marks as it does not have the simple dimension of time, but rather s^n, where n is the frequency power of the diffusion type CPE (n is close to 0.5). The relation between $R_{diff.} \cdot Y_0$ and the frequency of the maximum dispersion, f_{max}, is presented in Apendix B. This indicates the same basic process for diffusion on all three electrolyte/electrode combinations, but with different scaling factors (possibly different diffusion length).

***Table** 7 Comparison of the 'time constants' associated with the diffusion type (RQ) circuit, pO_2= 0.2 atm, T= 705-710 °C. The value of n in the dimension of τ is between 0.5 and 0.6.*

electrode	$R_{diff.}$ [Ω]	$Y_{0,diff.}$ [S·s^n]	$\tau_{diff.}$ [s^n]
gold	24	0.030	0.72
platinum	124	0.0063	0.78
silver	58	0.014	0.81

On the low frequency side of the impedance spectrum the contribution of another (RQ) combination can be observed (Au-electrode: figure 20, Pt-electrode: figure26 and Ag-electrode: figure 28). The resistance, $R_{lf.}$, seems to show a maximum around $pO_2 \approx 0.05$ atm (see figure 21). It can also be inferred from these figures that the time constant associated with this sub-circuit is around 1000 sec. (at 710°C) and increasing with decreasing pO_2. The impedance spectra measured under different levels of electrode polarisation (Apendix A.1 and A.2) indicate that this sub-circuit too is dependent on the polarisation level. The low accuracy of the data at low frequencies, however, precludes a detailed analysis. One important aspect is the large values observed for the CPE element in this circuit, about 2 F for the gold electrode and 17 F for the silver electrode. This indicates that the (pseudo-) capacitance is of a chemical nature and possibly connected with stoichiometry changes in the BiCuVOx bulk. The activation energies for the circuit parameters are quite high, 280-300 kJ·mol^{-1}, see Table 2. Within the experimental error the activation energies for $R_{lf.}$ and $Y_{0,lf.}$ are identical.

The high frequency (RQ) circuit could not be determined with accuracy. Its contribution to the electrode dispersion was, in most of the cases, rather small. Hence this part of the dispersion will not be considered further.

An interesting aspect is the observation of a 'negative'(*RC*) contribution to the dispersion. Although not at all obvious from visual inspection of the impedance diagrams, this contribution became apparent from a thorough analysis of the spectra. It was also found to be consistently present in all spectra, although sometimes the inaccuracy of the low frequency data made it impossible to establish the parameter values. For the gold electrode the temperature dependence of this sub-circuit could be measured with reasonable accuracy (see figures 24 and 25), leading to activation energies of around 38 kJ·mol^{-1}, about equal to the activation energie for the ionic conductivity of BiCuVOx, as observed from the high frequency real axis cut-off in the impedance spectra, $R_{electrolyte}$. A tentative explanation for the occurrance of this negative (*RC*) circuit will be presented in paragraph 4.3.1.

For both the gold and the silver electrode an estimate was made of the total electrode impedance (*dc*-value) as function of temperature (at pO_2=0.2 atm.). The apparent activation energy of the overall electrode process was obtained from an Arrhenius plot [11]. The corresponding activation energies are 140 (gold) and 125 kJ·mol^{-1} (silver), quite comparable to values obtained for erbia-stabilized bismuth oxide [3-5]. The overall value for the gold electrode is somewhat higher than found for only just the diffusion resistance, $R_{diff.}$. The total electrode resistance is the sum of many activated processes, hence the obtained activation energies must be regarded as 'apparent'.

A final remark should be made about the observed time dependence of the electrode impedance after a step in the pO_2 from 0.05 atm. to less than 0.01 atm.(silver electrode, see figure 29). As can be seen from Table 5, that the 'time constant' associated with $(RQ)_{diff.}$ virtually does not change with time while the resistance, $R_{diff.}$, steadily decreases and the Y_0-paremeter of the *Q*-element steadily increases. This indicates that the mechanism remains unchanged, but that a scaling parameter affects the magnitude. Based on the suggestions presented above, one could view this as the influence of the bulk-electron concentration, which slowly increases with time upon the step wise decrease in pO_2. Unfortunately, the actual value of the ambient pO_2 has not been measured during these experiments, so the influence of an oxygen partial pressure changing with time cannot be ruled out. Also, as it is assumed that some kind of reaction (dissolution) between the silver and the BiCuVOx had taken place, this behaviour is not necessarily representative for 'pure'BiCuVOx.

4.2.2 High temperature I-V characteristics

In 'wet' electrochemistry *reversible* electrode processes are generally modelled with the Butler-Volmer equation which relates the electrode current, *I*, to the electrode polarisation, η:

$$I = I_0\left[e^{\frac{\alpha_a F}{RT}\eta} - e^{-\frac{\alpha_c F}{RT}\eta}\right] \qquad (7)$$

This equation is based on the fundamental principle that both the oxidation reaction (cathodic direction) and the reduction reaction (anodic direction) occur simultaneously. At equilibrium (η=0) the fluxes of the reacting species are equal and of opposite sign (= I_0). In the anodic region the applied polarisation (i.e. a change in the 'electrochemical potential' of the electrons) will enhance the oxidation reaction and decrease the reduction reaction (and visa versa for the cathodic direction), resulting in a net current. For a simple one electron transfer reaction (e.g.: $Fe^{3+}_{aq.} + e \rightleftharpoons Fe^{2+}_{aq.}$) the sum of α_a and α_c is 1. For more complicated reactions with several reaction steps other values can be found [12]. The sum of the charge transfer coefficients is then given by: $\Sigma\alpha = n/\nu$, with *n* the number of electrons transferred *in* and ν the stoichiometry number *of* the rate determining reaction step. The transfer coefficients are obtained from the slope of log*I* versus η (Tafel-plot) in the cathodic or anodic domain where the current is dominated by either the cathodic or anodic flux. Hence for complicated systems the values of the charge transfer coefficients can be used in the elucidation of the reaction mechanism at the electrode.

One advantage of electrode studies in the liquid state is that the electrode reaction generally takes place homogeneously across the electrode surface. For solid electrolyte / electrode / gas phase systems the electrode reaction is, at least partially, confined to the triple phase boudary line (*TPB*), i.e. the line where the electrode, the electrolyte and the gas phase meet. Obviously the electrode reaction cannot take place at just a line. There will rather be a 'reaction zone' with an extension over a certain distance from

the triple phase boundary line. When the reaction zone extends over the electrolyte/ambient interface the active area will be determined by the diffusion rate of the electrons (or electron holes), hence by the electronic conductvity. When the reaction zone extends into the contact area between electrode and electrolyte, the area of the reaction zone will be determined by the diffusion of oxygen species. In both cases it may be argumented that the overall electrode expression will be a summation of 'local' Butler-Volmer expressions, whose properties depend on the distance from the *TPB*. Modelling of the electrode polarisation can be complicated further by dissociation/adsorption/diffusion 'reactions' which take place on the electrode metal surface (e.g. dissociation of O_2 on Pt) or even on the electrolyte surface. In general the charge transfer coefficients will then have an 'apparent' character and only qualitative conclusions can be drawn from the analysis of the Butler-Volmer characteristics.

On the well known stabilized zirconia electrolytes the choice of electrode material has a significant influence on the electrode properties. This is related to the large difference in catalytic activity with respect to the dissociation of adsorbed O_2. Hence the electrode resistance for nobel metal electrodes on yttria stabilized zirconia (YSZ) increases in the series $R_{Au} > R_{Pt} > R_{ag}$. The difference can be larger than two orders of magnitude. For the doped bismuth oxides no significant difference was found between Pt and Au electrodes. The results presented here for the BiCuVOx electrolyte fit quite nicely with this latter observation.

For most electrolyte/noble metal electrode systems (e.g. the stabilized ceria, zirconia and bismuth oxides) the anodic direction (oxygen evolution) shows a distinctly lower overpotential than the cathodic direction, or in terms of the apparent charge transfer coefficients: $\alpha_a \gg \alpha_c$. For the noble metal electrodes on BiCuVOx we find in this study the reverse: a smaller polarisation level for cathodic currents than for anodic currents. Rough estimates for the Au and the Ag electrodes, obtained from the uncorrected Tafel plots, figures 33 and 36, leads to apparent values for $\alpha_a \approx 0.8\text{-}1.0$ and $\alpha_c \approx 1.1\text{-}1.3$. Also the gold electrode has a somewhat lower electrode resistance (higher exchange current density, see Table 6) than the platinum and the silver electrode, although the differences are quite small. These could well be ascribed to differences in the electrode morphology and to the possible reaction of the Ag with the BiCuVOx surface.

Still, at 735 °C there is considerable hysteresis in the *I-V* curves, even at a low scan rate of 25 $\mu V \cdot s^{-1}$. At a scan rate of 2 $mV \cdot s^{-1}$ again the effect of a change of 'oxygen stoichiometry' is visible, see figure 34. Hence this effect must be taken into account in the development of a model for the electrode reactions. The magnitude of the exchange current density, J_0, for the gold electrode on BiCuVOx in air compares well with literature values found for bismuth erbium oxide (BiEr25) [3,4]. Data are presented in Table 8. Two types of electrodes on BiEr25 are presented, a sputtered and annealed electrode with a morphology similar to the BiCuVOx/Au electrode (see figure 2) and a co-pressed gauze electrode (1024 mazes per cm^2) with a very open structure. It is important to point out that the *I-V* curves for the BiEr25 electrodes showed significantly less hysteresis than the BiCuVOx/Au electrodes, but the electronic conductivity of BiEr25 is also significantly less than for the BiCuVOx material.

Table 8 *Comparison of exchange current densities for the BiCuVOx/gold (735 °C) and the BiEr25/gold (720 °C) electrodes at a pO_2=0.2 atm. Activation energies are also presented.*

System	J_0 [$A \cdot m^{-2}$]	E_a, [$kJ \cdot m^{-2}$]
BiCuVOx/Au	30-35	140*
$BiEr25/Au_{sput}$	60	140
$BiEr25/Au_{gauze}$	200	125

* *obtained from impedance mesurements*

One interesting feature, common in the *I-V* curves for the platina and silver electrodes (figures 35 and 36) is the occurrance of a current step with hysteresis which occurs in the anodic branch. Although we cannot explain this behaviour, it points to a kind of 'first order phase change'. It might be possible that both the Pt and Ag electrodes have to some extend reacted with BiCuVOx, forming a new phase which is dependent on pO_2. However, with the information at hand this is highly speculative.

4.3 Model description

The nearly insignificant difference in response between the gold, platinum and silver electrodes on BiCuVOx sets this electrolyte material apart from the stabilized zirconia's or ceria's. In its behaviour many smilarities are found with the doped-bismuth oxide/gold electrode systems. From a detailed analysis of the relation between electrode response and electrode metal and -morphology it was concluded, for the bismuth oxide based systems, that the exposed electrolyte surface presented the active electrode area [5]. This notion was further strengthened by the comparison of the exchange current densities with surface oxygen exchange rate, r_S, which indicated a close relationship:

$$J_0 = 4Fr_S \qquad (8)$$

when both were measured at the same temperature and pO_2 From the analysis a qualitative model was derived which is presented here in figure 39.

When the electrode is at rest (equilibrium, 39-middle) there is a continuous exchange of gas phase oxygen (O_2) with adsorbed oxygen species (O^-_{ad}). The dissociation and desorption rates are equal and oposite, as depicted by the equal length arrows. It is assumed in this model that the dissociation rate is dependent on the concentraton of 'free' electrons at the surface.

A second exchange reaction exists between the absorbed oxygen species and the bulk oxygen, which also has a net flux of zero, as depicted by the equal length black arrows. The rate of this step, or serie of consecutive steps, will also depend on the electron concentration.

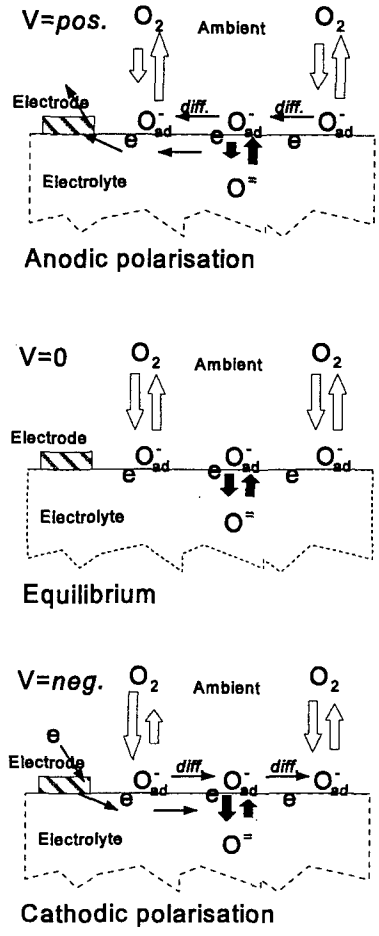

Fig. 39 Model for gas phase / electrode / electrolyte system with active gas phase exchange at electrolyte surface. Relative length of arrows indicate direction of net flux.

When the electrode is polarised in cathodic direction, i.e. injection of electrons into the electrolyte from the electrode, the exchange reactions are influenced, the reduction step will be favoured and the concentration of adsorbed oxygen species will increase at the electrode. Consequently a concentration profile of O^-_{ad} will develop from the electrode out, influencing the exchange process ocross the open electrolyte area (39-bottom). At the same time a concentration profile of electronic charge carriers in the bulk (presumably near the surface) will start to build up.

For a polarisation in the anodic direction the same picture, but in opposite direction, will emerge as indicated in the top part of figure 39. In a rather qualitative way, this model can explain the effects seen in the impedance spectra measured for the BiCuVOx/metal electrodes. A change in the pO_2 of the ambient will change the oxygen concentratio in the BiCuVOx and hence the concentration of free electrons or electron holes. A quite strong dependence on pO_2 was observed for the main dispersive element, Q_{diff}, for all three electrodes, indicating a strong connection with the concentration of electronic charge carriers. Furthermore, the resistance, R_{diff}, has the apperance of a charge transfer resistance (see figures23 and 31), which in this tentative model becomes a 'distributed'charge transfer resistance. The slope of the dependence seems to suggest a clear connection with electronic charge carriers. It is quite tempting to ascribe the observed diffusion element, Q_{diff}, to the diffusion of charged oxygen species across the BiCuVOx surface under influence of a concentration gradient. A more thorough study, however, of the electrode properties is needed in order to develop a proper model for this rather unique electrode process on a solid oxide oxygen conductor.

4.3.1 Model for 'inductive loop'

The so called 'inductive loops' in impedance spectra at intermediate and low frequencies have nothing to do with actual inductances. At high frequencies inductive behaviour is connected with the inductances of the current leads and, in case of measurements under potentiostatic control, the inductance (or combination of inductances) is caused by the current voltage converter. In fact the 'inductive loop' can be modelled by the combination of a negative resistance in parallel with a negative capacitance, a much more realistic interpretation which can be based on physical principles [13].

For electrodes under polarisation a negative (*RC*) contribution can be modelled by a stepwise charge transfer, combined with adsorbed intemediates [13,14]. At zero bias, however, no negative effect is predicted. In our case the negative effect is clearly observed for the electrodes at zero bias. A possible model for this behaviour can be derived from the surface diffusion model which has been described in the previous paragraph and in reference [5]. One should be aware of the fact that the reference electrode does not probe the gas phase oxygen partial pressure, but rather the equilibrium activity of an intermediate, adsorbed and charged oxygen species. Strong indications for this notion have been found by Bouwmeester et al. [15], who measured the electrode potential difference across a BiEr25 membrane in a pO_2 gradient. The measured potential difference at high oxygen flux rates was significantly less than predicted by the pO_2 difference. Although the BiEr25 sample does show some electronic conductivity, this was not high enough to explain the differences. The observed deviation from the theoretical Nernst potential difference could be ascribed to the slow dissociation and/or partial charge transfer of oxygen, which leads to an absorbed (charged) oxygen intemediate with an activity (equivalent to a oxygen partial pressure) which is different from the ambient pO_2.

When the working electrode is polarised in cathodic direction (negative potential with respect to the reference electrode) this may result in a decrease in concentration of the intermediate, absorbed oxygen species (here an O^-_{ad} species is assumed). The actual direction of the concentration change will depend on the relative magnitudes of the dissociation/desorption rates and the bulk transfer rates (see figure 39, open arrows, respectively black arrows). Through the surface diffusion process the O^-_{ad} concentration (or better: activity) at the reference electrode will also decrease, resulting in a smaller potential difference between working and reference electrode. The opposite will happen for an anodic polarisation.

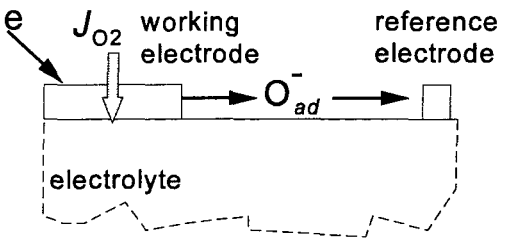

Fig. 40 *Schematic model of 'cross-talk' between the working electrode and reference electrode through surface diffusion of adsorbed oxygen species.*

When an ac-current is imposed on the electrochemical cell periodical anodic and cathodic polarisation will occur. When the frequency is high, the diffusion will be too slow to influence the oxygen activity at the reference electrode. When the frequency is very low with respect to the surface diffusion then the reference electrode potential will virtually follow the activity of the intermediate oxygen species at the working electrode. This will then counteract the voltage difference between the working and reference electrode which is due to the current flow from working to counter electrode, or in terms of impedances the 'electrolyte resistance' (or non-Faradaic resistance), $R_{electrolyte}$, will decrease from a high frequency value to a low frequency value.

Assuming a simple model, in which no exchange with the gas phase or the bulk occurs for the adsorbed O^-_{ad} species, a negative finite length diffusion element can be derived for this process [16]:

$$Z_{W-R}(\omega) = -Z_0 \frac{\tanh B\sqrt{j\omega}}{\sqrt{j\omega}} \qquad (9)$$

where B is related to the diffusion length and the inverse of the root of the diffusion coefficient. In the low frequency approximation the impedance can be represented by a *negative* parallel *RC* circuit. It can be argued that the negative resistance cannot become larger than the high frequency cut-off resistance,

$R_{electrolyte}$. It is interesting to note that $R_{neg.}$ remains smaller then $R_{electrolyte}$ over the entire temperature range (see figure 24).

Another explanation for the negative (*RC*) circuit could have been cross talk mediated through the gas phase, as at low frequencies considerably more oxygen is produced in the anodic half cycle, or consumed in the cathodic half cycle, than at high frequencies. This will cause an increase and a decrease in the oxygen partial pressure in the anodic and cathodic half-cycles of the electrode current at the working electrode. Through gas phase diffusion these effects will be noticeable at the reference electrode. Gas phase diffusion, however, is not a thermally activated process.

5 Conclusions

- The electrode response of the BiCuVOx/noble metal electrode system is not sensitive to the catalytic properties of the noble metal for oxygen adsorption and dissocation. The electrode response is quite similar to erbia doped bismuth oxide systems.
- At low temperatures (200° to 500°C) the electrolyte shows a significant change of oxygen activity (concentration) under polarisation. This slow change is due to the small but noticeable electronic conductivity. This bulk polarisation counteracts the electrode polarisation.
- At high temperatures (700°-735°C) the *ac*-electrode response is dominated by a diffusion process. This diffusion process is strongly dependent on the oxygen partial pressure and on the polarisation level, with an increase in the diffusion rate with decreasing pO_2 or cathodic polarisation.
- The resistance parallel to the diffusion element, i.e. in the (*RQ*) sub-circuit, shows the characteristics of a charge transfer resistance.
- Even at high temperatures hysteresis is observed in the polarisation curves of the electrodes. Changes in oxygen non-stoichiometry under polarisation is still noticeable.
- A 'negative loop' is a non-obvious, but consistent part of the impedance spectra. It can tentatively be explained by a 'cross-talk' between working electrode and reference electrode, possibly mediated by adsorbed and charge oxygen species.
- The *ac*-electrode response can be modelled with an equivalent circuit which contains several 'time constants'or dispersive sub-circuits. Assignment to specific surface and electrode processes is, t this time, highly speculative. The dominant diffusion sub-circuit, however, can be explained tentatively by a qualitative model in which the electrolyte surface is active in the exchange of oxygen.

- For a BiCuVOx based oxygen pump, operating at moderate temperatures (300°-500°C), it will be essential to find electrode materials that are highly active for oxygen adsorption and dissociation, e.g. mixed conducting perovskites.

6 Suggestions for future research

The results presented in this report provide a solid starting point for future research on the BiCuVOx materials. For the continuation two distinctly different directions can be discerned. One is centred on the technological aspects of an intermediate (200 - 400°C) oxygen pump unit which is based on the BiCuVOx solid electrolyte. The other, more fundamental study, is particularly focussed on the surface oxygen exchange process in BiCuVOx and on the influence of the concentration of mobile electrons (or electron holes) on the exchange rate and the electrode processes.

For the technological developments the emphasis should be on finding suitable electrode materials with high oxygen transfer rates. Of particular interest are the Perovskite type cobaltates and cobaltate-ferrates (e.g. the $La_{1-x}Sr_xFe_yCo_{1-y}O_{3-\delta}$ compound family [17]). The main concerns then are:

- The chemical and mechanical compatibility of these materials with BiCuVOx. When a successful combination has been obtained, further research efforts will focus on the optimisation of the electrolyte/electrode interface and the electrode/ambient interface.
- Development of cermet like electrode structures, i.e. porous ceramics of finely grained and percolatively mixed electrolyte and electrode materials.
- Development and optimisation of electrode deposition processes and techniques will form an important subject in this investigation.

Fundamental understanding of the oxygen transfer processes on the BiCuVOx/ambient interface, as well as the BiCuVOx/mixed conductor interface is needed in order to explain technological problems and results, or to make well founded predictions on the possible success of future research strategies. In my view the best way to proceed is by focussing on three targets:

- Study of the defect structure of BiCuVOx, in particular the relation between oxygen partial pressure, oxygen non-stoichiometry and the electronic conductivity. This would involve the study of the thermodynamic properties of BiCuVOx, e.g. measurement of 'oxygen titration curves' as function of temperature, see e.g. Lankhorst et al. [18,19].
- Study of the surface oxygen exchange rate by ^{18}O-isotope exchange [1,2,5]. This will provide more detailed information on the oxygen dissociation and -incorporation rate as function of oxygen partial pressure and temperature. These values will be of great importance for the study of the electrode processes on BiCuVOx.
- Study of electrode processes with stable gold electrodes with different patterns, using electrochemical impedance spectroscopy and current-voltage measurements as function of temperature and oxygen partial pressure. This should eventually lead to the development of a new theoretical model for the electrode response of an electrolyte with a surface which is active in the oxygen dissociation and exchange [5].

Our research group is especially capable of performing the fundamental research aspects mentioned above. But also the more technological aspects are gaining our attention. It is important to note that recently we have become engaged in the fundamental and technological research of composite materials with special properties.

List of symbols

α_a	anodic charge transfer coefficient
α_c	cathodic charge transfer coefficient
η	actual electrode potential with respect to reference (rest) potential
τ	time constant [s] (only for a (*RC*) combination)
ω	radial frequency [rad·s^{-1}]
B	argument factor of Tanh() function [s$^{1/2}$]
C	capacitance [F]
D	diffusion coefficient [m ^{2}·s^{-1}]
E_a	activation energy [J·mol^{-1}]
I	current [A]
I_0	exchange current [A]
j	$\sqrt{-1}$
J_0	exchange current density [A·m^{-2}]
f	frequency [Hz]
F	Faraday constant [Coulomb·mol^{-1}]
n	power of radial frequency
pO_2	partial pressure of oxygen [atm.]
Q	short notation for CPE
R	gas constant [J·K^{-1}·mol^{-1}]
R	resistance [Ω]
$R_{electrolyte}$	non-Faradaic resistance in three-electrode cell [Ω]
T	absolute temperature [K]
V	voltage [V]
W	Warburg or semi-infinite diffusion element
$Y(\omega)$	admittance (= $Z(\omega)^{-1}$) [S]
$Y_{CPE}(\omega)$	admittance function of constant phase element
Y_0	magnitude of a CPE (*q*-element) [S·s^n]
$Z(\omega)$	impedance [Ω]

References

[1] B.A. Boukamp, K.J. de Vries and A.J Burggraaf, '*Surface oxygen exchange in bismuth oxide based materials*', in J. Nowotny and W. Weppner eds '*Non-Stoichiometric Compounds; Surfaces, Grain Boundaries and Structural Defects*', (Kluwer, Dordrecht) 1989, p299-309.

[2] B.A. Boukamp, I.C. Vinke, K.J. de Vries and A.J. Burggraaf, '*Surface oxygen exchange kinetics of solid oxide ion conductors*', in '*Fast Ion Transport in Solids*', eds B. Scrosati, A. Magistris, C.M. Mari and G. Mariotto, NATO ASI Series, Series E: Appl. Sci. **Vol. 250** (Kluwer Academic, Dordrecht, 1993) pp 167-180.

[3] I.C. Vinke, B.A. Boukamp, K.J. de Vries and A.J. Burggraaf, '*Three-Electrode Current-Voltage Measurements on Erbia-Stabilized Bismuth Oxide with Sputtered Noble Metal Electrodes*', Solid State Ionics **51** (1992) 249-259.

[4] I.C. Vinke, B.A. Boukamp, K.J. de Vries and A.J. Burggraaf, '*Three-Electrode Current-Voltage Measurements on Erbia-Stabilized Bismuth Oxide with Co-Pressed Gold Gauze Electrodes*', Solid State Ionics **58** (1992) 33-40.

[5] B.A. Boukamp, B.A. van Hassel, I.C. Vinke, K.J. de Vries and A.J. Burggraaf, '*The oxygen transfer process on solid oxide/noble metal electrodes, studied with impedance spectroscopy, dc-polarization and isotope exchange*' Electrochimica Acta, **38** (1993) 1817-1825.

[6] B.A. Boukamp, '*Pt and Au electrodes on BiCuVOx*', Internal report 97340/CT31/bab, University of Twente (1997).

[7] B.A. Boukamp, '*A package for impedance/admittance analysis*', Solid State Ionics **18-19** (1986) 136-140.

[8] B.A. Boukamp, '*A non-linear least squares fit procedure for analysis of immittance data of electrochemical systems*', Solid State Ionics **20** (1986) 31-44.

[9] B.A. Boukamp, *'A Linear Kronig-Kramers Transform Test for Immittance Data validation*', J. Electrochem. Soc., Vol. 142 [6] (1995) 1885-1894.

[10] M. Verkerk, *Electrical conductivity and interface properties of oxygen ion conducting materials*', Thesis, Twente University, 1982.

[11] S. Ladet and B.A. Boukamp, '*Comparison between BiCuVOx/Pt, BiCuVOx/Au and BiCuVOx/Ag*', Internal report 97687/CT31/SL, University of Twente (1997).

[12] J.O.M. Bockris and A.K.N. Reddy, *Modern Electrochemistry*, Vol. 2., Plenum press (New York, 1970), Chapter 9.

[13] C. Gabrielli, '*Identification of electrochemical processes by frequency response analysis*', Technical report Nr. 004/83, Solartron Instrumentation Group, Farnborough (1984).

[14] B.A. van Hassel, B,A. Boukamp, A.J. Burggraaf, '*Electrode polarization at the Au, O_2 (g)/yttria stabilized zirconia interface. Part I: Theoretical considerations of reaction model*', Solid State Ionics 48 (1991) 139-154.

[15] H.J.M. Bouwmeester, H. Kruidhof, A.J. Burggraaf and P.J. Gellings, '*Oxygen semipermeability of erbia-stabilized bismuth oxide*', Solid State Ionics, Vol. 53-56 (1992) 460-468.

[16] B.A.Boukamp et al., *to be published.*

[17] J.A. Kilner, '*Isotopic exchange in mixed and ionically conducting oxides*', in Proc. of the 2nd Int. Symp. On Ionic and Mixed Conducting Ceramics, eds T.A. Ramanarayanan, W.L. Worrel and H.L. Tuller, Electrochemical Society Proceedings 94-12,(1995) 174.

[18] M.H.R. Lankhorst, J.E. ten Elshof, '*Thermodynamic quantities and defect structure of $La_{0.6}Sr_{0.4}Co_{1-y}Fe_yO_{3-\delta}$ (y=0-0.6) from high-temperature Coulometric titration experiments*', J. Solid State Chem.. 130 (1997) 302-10.

[19] M.H.R. Lankhorst, H.J.M. Bouwmeester and H. Verweij, '*High-temperature coulometric titration of $La_{1-x}Sr_xCoO_{3-\delta}$: Evidence for the effect of electronic band structure on nonstoichiometry behaviour*', J. Solid State Chem.. 133 (1997) 555-67.

Appendix A

A.1 Impedance diagrams of the gold electrode under polarisation

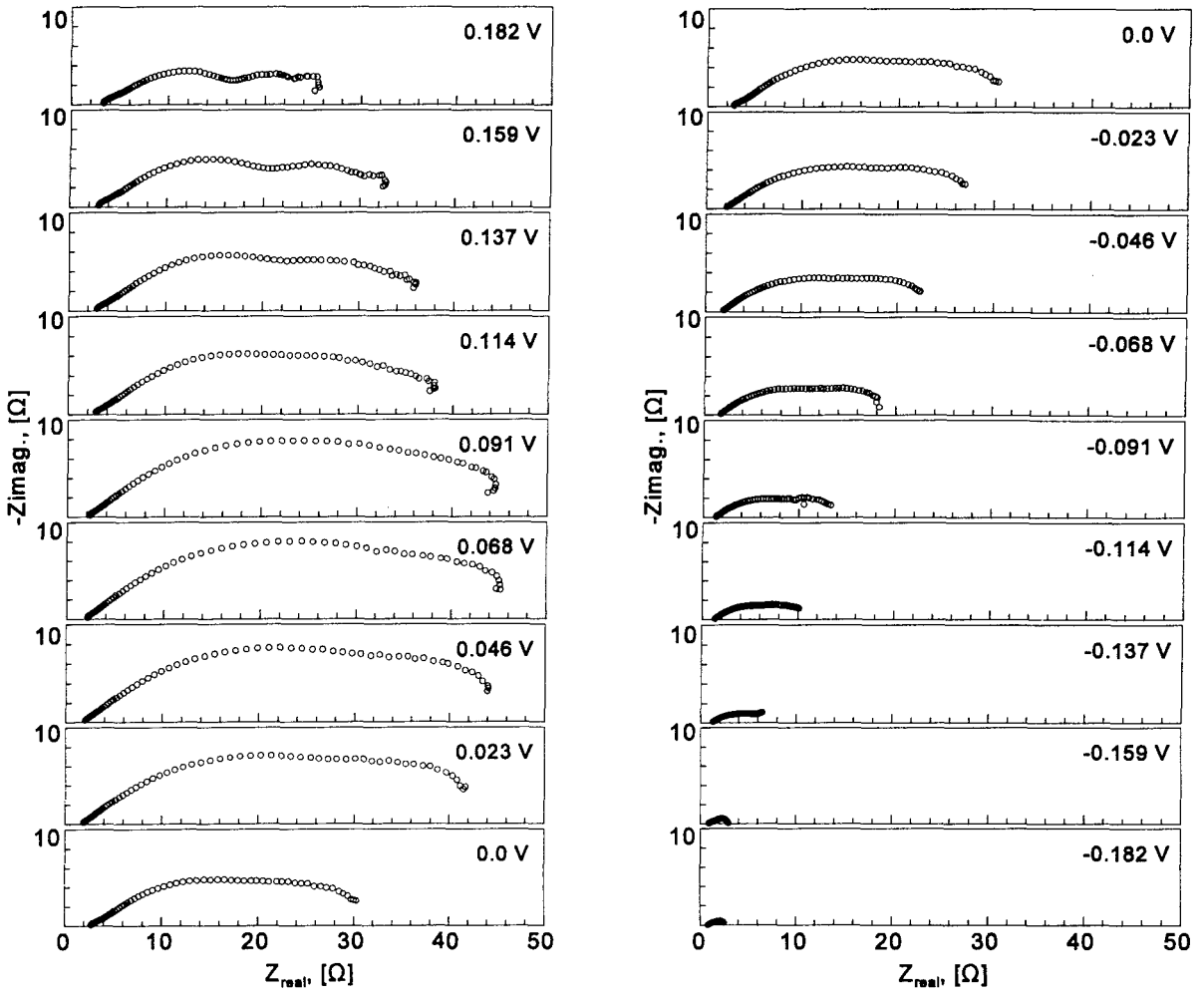

Fig. A-1 *Influence of electrode polarisation on the impedance of the Au-electrode. Polarisation level is indicated in each impedance diagram. On the left side anodic polarisation (oxygen evolution), on the right side cathodic polarisation (oxygen incorporation). Data measured at 710 °C and in 0.2 atm. pO_2. Frequency range: 1 mHz to 65 kHz.*

The overall electrode resistance of the BiCuVOx/Au,air electrode shows a clear maximum at positive (anodic, oxygen evolution) polarisation. The response of the BiCuVOx/Au,air electrode to the step change in the polarisation level is quite slow. This can result in a 'non steady state' situation during the impedance measurement, especially in the low frequency range (<0.1 Hz). In some of the impedance diagrams this is indicated by the 'curl' at the low frequency end. Kramers-Kronig transform test analysis [9] of the data confirms this observation. As a result the complete CNLS-analysis of these impedance spectra leads to rather scattered results, which is due to a rather strong coupling between the fit parameters (i.e. a limited spread on the time scale of the associated time constants, which is indicated by the more or less featureless apperance of the frequency dispersion).

A.2 Impedance diagrams of the silver electrode under polarisation

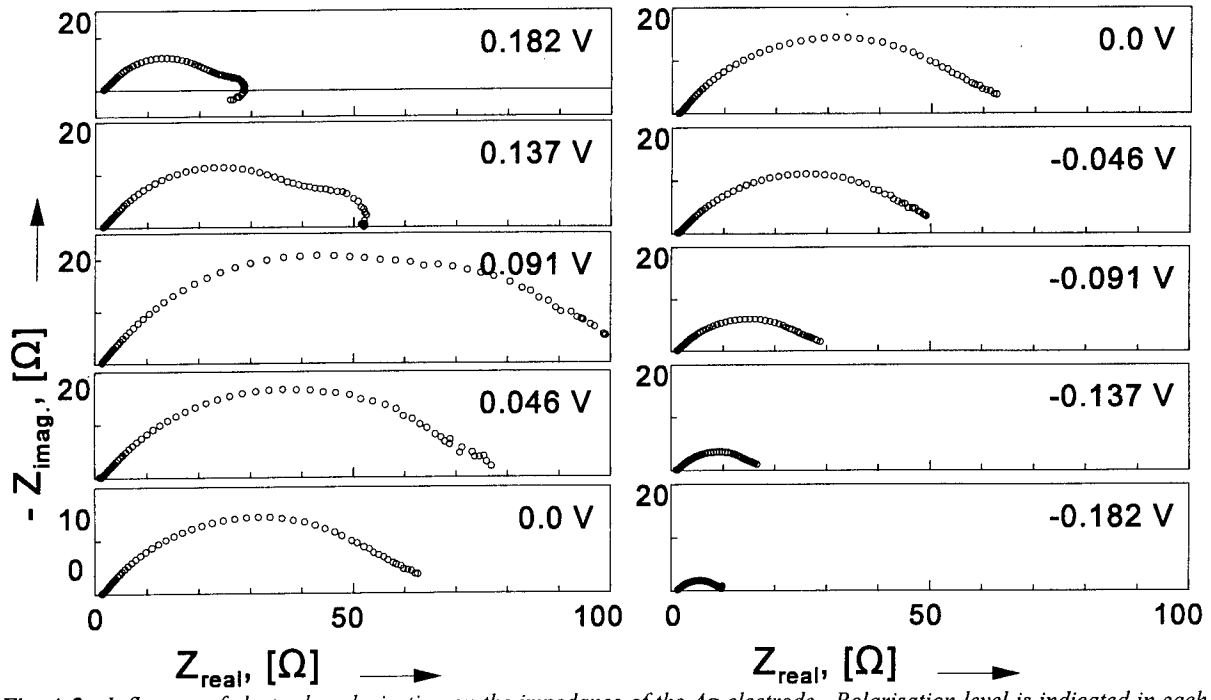

Fig. A-2 Influence of electrode polarisation on the impedance of the Ag-electrode. Polarisation level is indicated in each impedance diagram. On the left side anodic polarisation (oxygen evolution), on the right side cathodic polarisation (oxygen incorporation). Data measured at 705 °C and in 0.2 atm. pO_2. Frequency range: 1 mHz to 65 kHz.

The overall electrode resistance of the BiCuVOx/Ag, air electrode shows a clear maximum at positive (anodic, oxygen evolution) polarisation. This effect was also observed for the Au-electrode (figure A-1, previous page).

Appendix B

A parallel (RC) circuit has a time constant, τ_{RC}, associated with it, with $\tau_{RC} = R \cdot C$. This time constant is easily recognized as the decay time of an initial voltage across the (RC) circuit. This time constant is also associated with the frequency at which the absolute value of the imaginary part of the impedance shows a maximum. The impedance for a (RC) circuit is given by:

$$Z(\omega) = \frac{R - j\omega CR^2}{1 + (\omega CR)^2} \tag{B.1}$$

Hence the maximum in $|Z_{im}(\omega)|$ is found for $\omega CR=1$. With $\omega=2\pi f$ this results in $\tau_{RC} = (2\pi f_{max})^{-1}$, with f_{max} the frequency (in Hz) for which the maximum occurs.

For a parallel combination of a resistance and a CPE, (RQ), the time constant is not well defined and does not have the simple dimension of unit time. A pseudo time constant can be defined from the maximum in the impedance, analogue to the (RC) circuit. The full impedance expression is given by:

$$Z(\omega) = \frac{R + R^2 Y_0 \omega^n \cos\frac{n\pi}{2} - j\, R^2 Y_0 \omega^n \sin\frac{n\pi}{2}}{1 + 2\, RY_0 \omega^n \cos\frac{n\pi}{2} + (RY_0 \omega^n)^2} \tag{B.2}$$

The maximum in $-Z_{im}(\omega)$ is found from:

$$\frac{d}{d\omega} -Z_{im}(\omega) = \frac{nRY_0 \omega^{n-1} \sin\frac{n\pi}{2}\left(1 - (RY_0 \omega^n)^2\right)}{\left(1 + 2RY_0 \omega^n \cos\frac{n\pi}{2} + (RY_0 \omega^n)^2\right)^2} = 0 \tag{B.3}$$

from which it follows that $R\,Y_0\,\omega^n = 1$, or $\tau_{RQ} = R\,Y_0 = \omega^{-n}$. This results in a dimension of s^n for τ_{RQ}. The frequency for the maximum in $-Z_{im}(\omega)$, i.e. the top of the depressed semi-circle, is then given by:

$$f_{max} = \frac{1}{2\pi \sqrt[n]{RY_0}} \tag{B.4}$$

Distribution list

Dr. B.A. Boukamp
Dr. H.J.M. Bouwmeester
Prof. dr. ir. H. Verweij

University of Twente
Group Inorganic Materials Science
P.O. Box 217
7500 AE Enschede

Prof.dr. B. Dunn
Department of Materials Science and Engineering
University of California at los Angeles
6532 Boelter Hall
Los Angeles, CA 90095-1595
U.S.A.

(Successor to Capt. J.E. Fenner, USAF, BSC)
Armstrong Laboratory
AL/CFTS
2504 Gillingham Dr. Ste. 1
Brooks AFB, TX 782235-5104
U.S.A.

Dr. M.-S. Wong
Systems Research Laboratory at Brooks A.F.B.
Armstrong Laboratory
AL/CFTS
2504 Gillingham Dr. Ste. 1
Brooks AFB, TX 782235-5104
U.S.A.

European Office of Aerospace Research and Development
Attention: Mr. Guymon
Department of the Air Force
422nd ABS/CON
Bldg 202, Room 17
RAF Croughton, NORTHANTS
United Kingdom, NN13 5NQ

Maj. M.H. Smith
European Office of Aerospace Research and Development
223/231 Old Marleybone Road
London NW1 5H
United Kingdom